








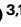
# Development policy affects coastal flood exposure in China more than sea-level rise

Received: 17 February 2025

Accepted: 21 August 2025

Published online: 24 September 2025

 Check for updates

Yafei Wang <sup>1,2,3,4</sup>✉, Yuxuan Ye <sup>1,2</sup>, Robert J. Nicholls <sup>5,6</sup>, Lennart Olsson <sup>3</sup>,  
Detlef P. van Vuuren <sup>7,8</sup>, Garry Peterson <sup>4</sup>, Yao He <sup>1,2</sup>, Manchun Li<sup>9,10</sup>,  
Jie Fan <sup>1,2</sup> & Murray Scown <sup>3,11</sup>✉

Effective coastal exposure assessments are crucial for adaptively managing threats from sea-level rise (SLR). Despite recent advances, global and regional assessments are constrained by omitting critical factors such as land-use change, failing to disaggregate potential impacts by land uses and oversimplifying land subsidence. Here we address these gaps by developing context-specific scenarios to 2100 based on a comprehensive analysis of Chinese coastal development policies. We integrate high-resolution simulations of population and land-system changes with inundation exposure assessments that incorporate SLR, land subsidence, tides and storm surges, offering a more nuanced understanding of coastal risks. Across our plausible set of downscaled scenarios of shared socioeconomic and representative concentration pathways, policy decisions have a bigger effect on what is exposed to coastal flooding until 2100 than does the magnitude of SLR. Hence, coastal policy decisions largely influence coastal risk and adaptation needs to 2100, demonstrating the necessity of appropriate policy design to manage coastal risks.

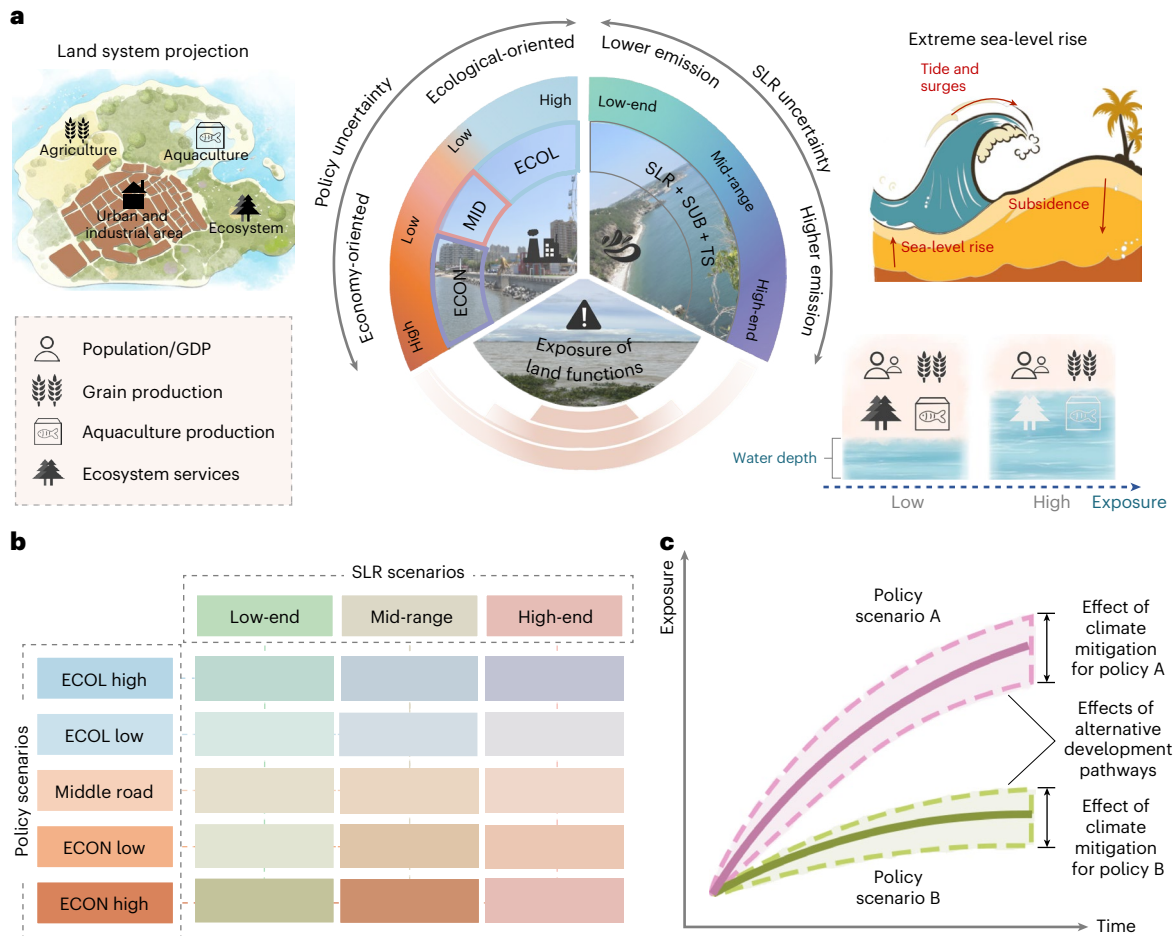
Coastal zones are on the front line when it comes to facing the increasing threats associated with climate change<sup>1–3</sup>. Coastal scenario analysis and risk assessments are important tools for advancing knowledge and guiding policy—providing, for example, estimates of populations and assets exposed to flooding<sup>4,5</sup> and weighing anticipated economic losses against costs of adaptation<sup>6</sup>. However, coastal risk is multifaceted. Climate change affects sea-level rise (SLR) and the frequency and intensity of storms, combining to raise extreme sea levels (ESLs) in certain areas<sup>7</sup>; land subsidence driven by human activity such as groundwater extraction increases relative SLR in populated coastal lowlands often at rates much higher than those caused by climate change alone<sup>5,8</sup>; and coastal development and adaptation actions

determine who and what are exposed and vulnerable to flooding, salinization or erosion.

So far, limited advances have been made in global and regional coastal inundation exposure assessments and management using the scenario frameworks of the shared socioeconomic and representative concentration pathways (SSPs and RCPs). They, for instance, mostly (1) do not disaggregate impacts on different land uses and sectors (see ref. 9 for recent advances in Europe); (2) do not consider all components driving exposure (see ref. 3); and (3) have coarse spatial resolution (see refs. 10,11 for recent improvements to the commonly applied dynamic and interactive vulnerability assessment (DIVA) modelling framework). Recent assessments for China have ignored the effects

<sup>1</sup>Key Laboratory of Regional Sustainable Development Modeling, Institute of Geographic Sciences and Natural Resources Research, Chinese Academy of Sciences, Beijing, China. <sup>2</sup>College of Resources and Environment, University of Chinese Academy of Sciences, Beijing, China. <sup>3</sup>Lund University Centre for Sustainability Studies (LUCSUS), Lund University, Lund, Sweden. <sup>4</sup>Stockholm Resilience Centre, Stockholm University, Stockholm, Sweden. <sup>5</sup>Tyndall Centre for Climate Change Research, University of East Anglia, Norwich, UK. <sup>6</sup>School of Engineering, University of Southampton, Southampton, UK. <sup>7</sup>PBL Netherlands Environmental Assessment Agency, The Hague, the Netherlands. <sup>8</sup>Copernicus Institute of Sustainable Development, Utrecht University, Utrecht, the Netherlands. <sup>9</sup>School of Geography and Ocean Science, Nanjing University, Nanjing, China. <sup>10</sup>Collaborative Innovation Center for the South Sea Studies, Nanjing University, Nanjing, China. <sup>11</sup>Swedish Centre for Impacts of Climate Extremes (CLIMES), Lund University, Lund, Sweden.

✉e-mail: [wangyafei@igsrr.ac.cn](mailto:wangyafei@igsrr.ac.cn); [murray.scown@lucsus.lu.se](mailto:murray.scown@lucsus.lu.se)



**Fig. 1 | Improved coastal exposure assessment framework covering several components.** **a**, We combine land-system change affected by coastal development policies alongside mean SLR, land subsidence (SUB), and tides and storm surges (TS). **b**, We combine the effects of ECON, ECOL and MID policy scenarios with enhanced relative SLR scenarios spanning the broad set of SSP-RCP scenarios and including land subsidence. **c**, We evaluate potential impacts to several land-system functions, as well as population and GDP, by considering

potential flood exposure to different water depths over time under different scenarios. Policy scenarios have a median effect on exposure (solid lines), around which SLR scenarios create uncertainty (shaded bands). Similarly (though not illustrated), SLR scenarios have a median effect around which policy scenarios create uncertainty. The combined analysis reveals the sensitivity of exposure outcomes to both policy decisions and climatic trajectories.

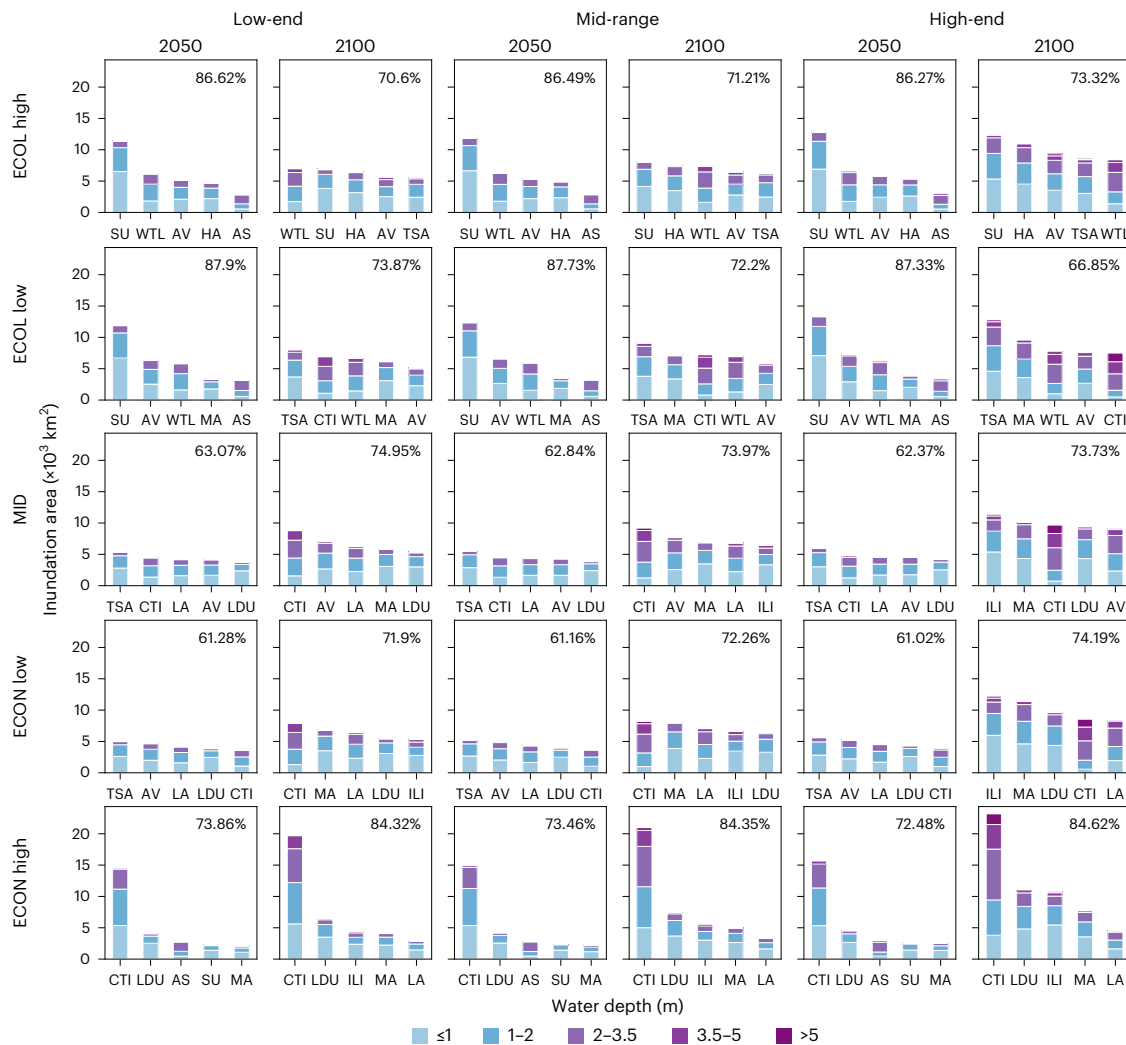
of land subsidence<sup>12,13</sup> or have failed to consider in detail how land-use planning and development dynamics interact with SLR to affect coastal exposure<sup>8,10</sup>. Such omissions could result in underestimates of exposure and/or overemphasis on climate change and SLR as its main driver, leading to misjudgments in the urgency of adaptation and/or confusion as to which actors have agency and responsibility.

Here we assess how Chinese coastal development plans interact with relative SLR and extreme events to determine exposure of several coastal zone functions across a range of scenarios. This is done by simulating land-system changes for the entire coastal zone of mainland China and Hainan for five development policy scenarios and combining this with estimates of land subsidence and ESLs across three SLR scenarios. For the land-use and population scenarios, we use the CLUMondo model to spatially simulate future land-system changes based on an analysis of 114 national and provincial coastal zone plans and policies. The scenarios capture policy elements that are oriented towards economic development (ECON), ecological protection (ECOL) or the middle road (MID). For the ECON and ECOL scenarios, we also considered variants that differ in the intensity of the policies applied. The subsequent inundation exposure assessment advances previous attempts by including all relevant components (SLR, land subsidence and tides and storm surges) and an improved geometric inundation model that considers spatial connectivity and attenuation (Fig. 1).

Extreme events have the greatest effect on potential inundation area, with land subsidence and SLR amplifying the effect. However, coastal development scenarios have a greater effect on which land-system functions are exposed than do SLR scenarios. These findings indicate that disaster preparedness, land-subsidence mitigation and improved adaptation planning are the most important measures for coastal flood risk management in China, to be complemented by emissions reductions that will reduce the SLR effect globally, as well as along China’s coastline. Our findings also suggest that the set of futures in the SSP-RCP framework used for global and regional scenario analyses does not cover the full range of possible futures that can be shaped by local and national policies. Our approach enables the integration of development policies and land-system change into the analysis and could be used to explore detailed coastal adaptation scenarios in future work in China and elsewhere.

**Results**

China has been subject to coastal flooding due to tide/storm surge effects throughout its history and large areas are currently threatened by flooding and depend on defences to maintain current functions<sup>10</sup>. Our high-resolution disaggregated analysis reveals that future exposure of different coastal zone functions depends not only upon the SLR scenario, but largely also on the policy pathways. Land-system



**Fig. 2 | Inundation areas of the top five exposed land-system types by water depth.** The land-system types are shown under different policy and SLR scenarios in 2050 and 2100, assuming current flood protection standards and an interactive effect of 10% of SLR on extreme events. Columns from left to right show the SLR scenarios of low-end (2050 and 2100), mid-range (2050 and 2100) and high-end (2050 and 2100). Rows show policy scenarios. The percentage value in each panel

indicates the fraction of the total inundation area represented by the top five land systems shown. Land-system abbreviations: AS, aquaculture system; AV, agricultural hinterland village; CTI, coastal industrial area; HA, high-intensity agricultural area; ILI, inland industrial area; LA, low-intensity agricultural area; LDU, low-density urban area; MA, medium-intensity agricultural area; SU, suburban area; TSA, towns and semi-dense areas; and WTL, wetlands.

changes vary greatly across policy pathways (Supplementary Note 1 and Extended Data Fig. 1) and, under all SLR scenarios, a transition in coastal policy from strictest ecological protection (ECOL high) to most aggressive economic development (ECON high) dramatically increases the development intensity of urban and industrial land exposed to flooding (Fig. 2). The top land-system types exposed shifts from suburban area, agriculture-hinterland village, high-intensity agriculture area and wetlands in the ECOL high scenario to coastal and inland industrial areas and low-density urban areas in the ECON high scenario (Fig. 2). This indicates that impacts, should flooding occur, will not happen uniformly across all land systems (as aggregated gross domestic product (GDP) calculations assume) and that it is the policy scenario and not the SLR scenario that mostly determines which land-system types will be exposed.

By contrast, the SLR scenario influences the total inundation area and depths in different land systems (Fig. 2, Extended Data Figs. 2–4 and Supplementary Note 2). By 2100, the area potentially exposed to inundation under ESLs could reach 29,290 km<sup>2</sup> (5.84% of the analysed coastal zone) in the low-end scenario; 34,400 km<sup>2</sup> (6.86%) in the mid-range; and 49,370 km<sup>2</sup> (9.85%) in the high-end scenario, assuming

current flood protection standards and an interactive effect between climate change and extreme events equal to 10% of SLR (CCE<sub>10</sub>; Methods). The overwhelming majority of the potential inundation extent is driven by tides and storm surges (that is, extreme events), while SLR alone and in combination with land subsidence are not high enough to exceed current protection standards anywhere along the coast (Extended Data Fig. 4). When considering no flood protection, the effect of land subsidence on inundation extent by 2100 is over 14 times that of SLR alone in the low-end scenario and about 1.5 times greater in the high-end scenario (Extended Data Fig. 4). The largest effect on inundation extent caused by increasing the magnitude of interaction between SLR and extreme events is about 17% in 2100, with current protection (Extended Data Fig. 4 and Supplementary Note 2). The presence of flood protection reduces the maximum potentially inundated area in 2100 by around 18–19% compared with no protection, depending upon scenario, but the relative patterns remain very similar (Supplementary Note 3).

To gauge the potential impacts of flooding on different land-system functions in China’s coastal zone, we calculated five indicators within the potentially inundated areas: (1) human population,

(2) monetary value of ecosystem services, (3) grain production, (4) (terrestrial) aquaculture production and (5) GDP. The first four of these were calculated from spatial simulations using CLUMondo, while GDP was calculated on the basis of the contribution of each land system to total GDP in the coastal zone (although we did not use discount rates, so future absolute values should be considered underestimates). Our assessment indicates a complicated interaction between development policy scenarios and their effect on land-system patterns, on the one hand, and SLR scenarios and their interaction with land elevation, on the other.

Population and GDP exposure are, unsurprisingly, highest in the high-end SLR scenario and ECON high policy scenario (Fig. 3a,b,m,n and Extended Data Figs. 5 and 6). Population exposure increases in the coming decades under all scenarios. This is despite continual declines in total coastal zone population from 2020 onwards in the ECOL and MID policy scenarios (Supplementary Table 2), indicating population concentration in exposed areas near the coastline. Most scenario combinations show a slight decline in population exposure towards the end of the century due to population decline (Fig. 3a,b). By contrast, exposure of GDP continues to rise under all scenarios even at the end of the century (Fig. 3m,n). When considering the results for a 10% interaction between SLR and extreme events and assuming current flood protection standards: by 2050, 6.8% (ECOL high | low-end) to 8.9% (ECON low | high-end) of the population and 7.5% (ECOL low | low-end) to 12.1% (ECON high | high-end) of GDP, within our delineated coastal zone will be exposed to inundation. By 2100, these ranges increase to between 9.5% (ECOL low | low-end) and 19.1% (ECON high | high-end) for population and 11.9% (ECOL low | low-end) to 22.2% (ECON high | high-end) for GDP.

In terms of food, grain production exposure is consistently higher under the ECOL and MID scenarios than the ECON scenarios (Fig. 3h and Extended Data Fig. 7). Between 4.0% (ECON high | low-end) and 7.4% (ECOL low | high-end) of grain production in the coastal zone could be exposed by 2050; again assuming current protection and a 10% SLR interaction with extreme events. These fractions increase to 5.8% (ECON high | low-end) and 13.5% (ECOL low | high-end), respectively, by 2100. Aquaculture is exposed to much greater inundation depths than all other land-system functions we analysed (Extended Data Fig. 8). As much as 19.2% (ECOL low | high-end) of aquaculture production in the coastal zone could be exposed to inundation depths of 2 m or more by 2050. Exposure of aquaculture production peaks around 2050 in all policy scenarios, then declines towards 2100 (Fig. 3k). However, as inundation depth and extent continue to increase under high-end SLR, as much as 11.9% of aquaculture production will be exposed to inundation depths of 3.5 m or more in the ECON low scenario (Extended Data Fig. 8). In contrast to grain, aquaculture exposure is consistently highest under the ECON high development scenario (Fig. 3k).

Exposure of absolute ecosystem services value (ESV) is consistently higher in the ECOL policy scenarios, while the MID and ECON scenarios are similar (Fig. 3h). Between 5.8% (ECON high | low-end) and 7.2% (ECOL high | high-end) of monetary ESV in the coastal zone is projected to be exposed by 2050 (with same assumptions as above). By 2100, ECON high | high-end has the highest proportional exposure (13.7%) with ECOL high | low-end the lowest (8.2%). In our calculations, ESV is higher in natural ecosystems than in others and these may tolerate some level of inundation—particularly wetlands, for example—so the depth (Extended Data Fig. 9) and duration of inundation of ESV may be important to consider.

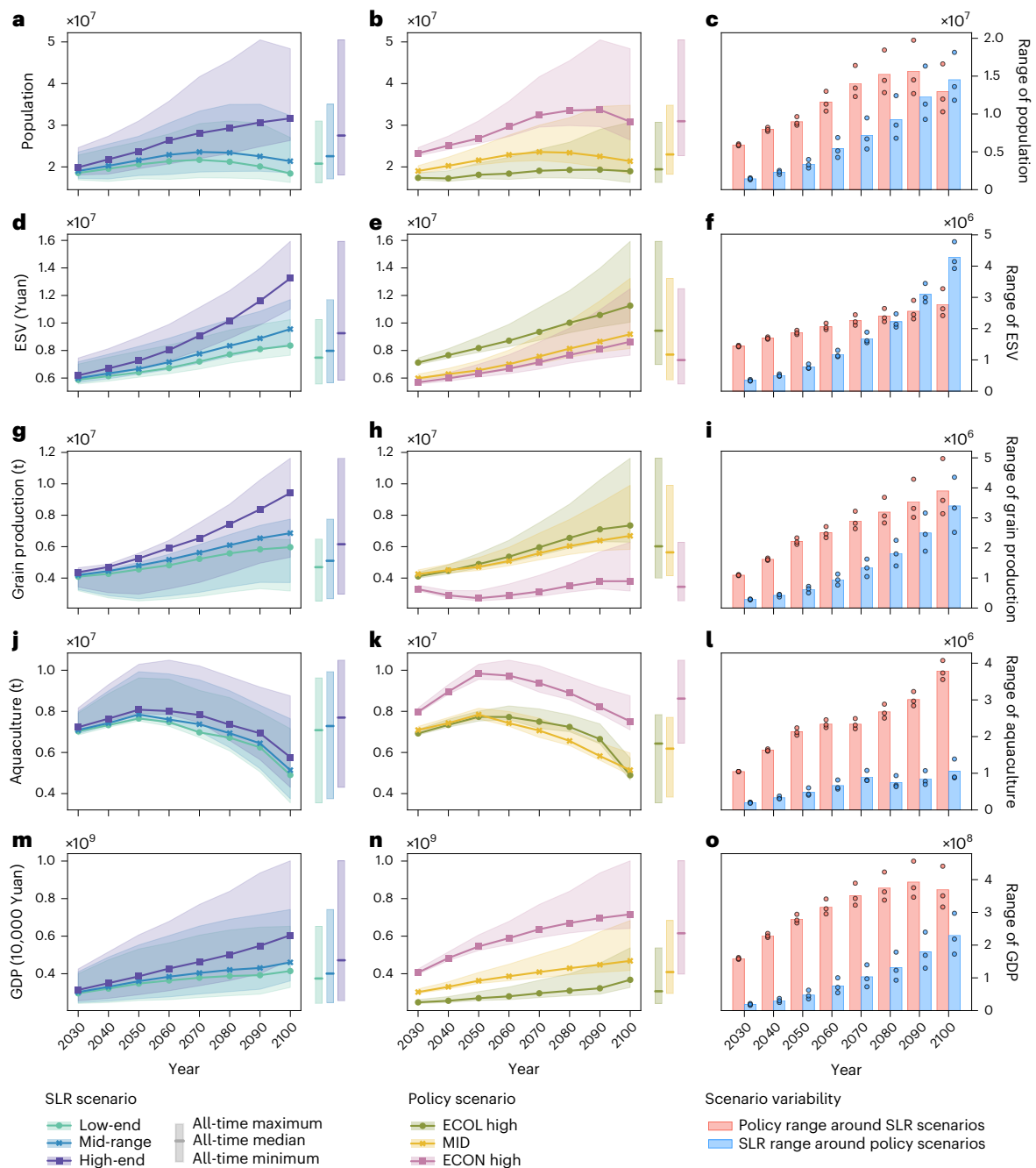
Our analyses enable us to determine whether policy scenarios or SLR scenarios have a greater effect on the potential impacts on different coastal zone functions. For population and grain production exposure to flooding, the sets of SLR and policy scenarios show increasingly similar ranges by the end of the century (Fig. 3a–c,g–i), indicating relatively similar long-term influences of policy and SLR scenarios on exposure, although development uncertainty caused by different

policies plays a much larger role in the coming decades (Fig. 3c,i). The increased role of development policy is also evident for aquaculture and GDP exposure and this continues at least until 2100 (Fig. 3j–o). The effect is particularly large for aquaculture (Fig. 3l). By contrast, from 2090, variation in ESV exposure depends more on the SLR scenario than on the policy scenario (Fig. 3f). Regionally, in the three strategic zones in China, the Bohai Rim and Greater Bay display even greater effects of policy scenarios on exposure, whereas the Yangtze River Delta displays a much greater effect of SLR scenarios for exposure of population, GDP, grain production and ESV by the end of the century (Extended Data Figs. 3 and 10).

## Discussion

Our analysis unpacks the differential effects of the various factors contributing to coastal flood exposure. Whether changing exposure is driven mainly by land subsidence, SLR or development in the floodplain, for example, determines what the best management strategy might be and who has agency and responsibility for that strategy. Our results reveal that inundation exposure of land in China is mostly affected by ESLs associated with tides and storm surges. These are natural phenomena, although climate change and higher seas are expected to amplify them in certain areas and reduce them in others<sup>7,14,15</sup>. Adaptation measures such as early-warning systems, floodplain zoning and/or flood protection measures are necessary to deal with extreme events. Ecosystem-based approaches, such as seagrass meadows and mangroves, may be effective in buffering storm surges and reducing their energy<sup>16,17</sup>, including hybrid approaches combined with dikes. In certain places along the Chinese coast, land subsidence happens much faster than mean SLR, exacerbated by groundwater extraction, dense construction and disconnection of alluvial plains from river flooding and sedimentation. Regulating groundwater extraction is essential to mitigate and avoid worst-case-scenario land subsidence, particularly in deltas<sup>18</sup>. Sedimentation enhancement strategies are also promising adaptation solutions in deltas<sup>19,20</sup>, although may be limited in highly developed areas where land is fully used and temporary flooding with sediment-laden water is not appropriate. China, being among the world's highest GHG-emitting countries, also has a great deal of agency and responsibility when it comes to mitigating climate change and associated SLR, so emissions reductions are also in the country's best interest when it comes to minimizing coastal risk up to and beyond 2100.

Beyond the physical determinants of relative SLR and extreme events, coastal development also drives flood exposure<sup>2</sup>. Our results reveal that for certain land functions, exposure is determined more by how the Chinese coastal zone is developed than by the magnitude of SLR. China's coastal land development tends to expand towards the shoreline and land reclamation is common, but policies focused on economic or ecological priorities will substantially influence what is potentially exposed. For at least the next 50 years, the range across the government's existing planning policies surpasses the differences between various global climate models. Thus, policy-makers have a great deal of agency in mitigating risk through land planning, particularly in strategic areas (Extended Data Figs. 3 and 10), as well as through emissions reductions. We recommend our integrated assessment findings be incorporated into China's medium- and long-term development strategies as a critical scientific basis for coastal planning at all levels. Specifically, these results should inform urban master planning, the delineation of ecological protection redlines and the approval of land-use changes. At the subnational level, coastal provinces and prefecture-level cities should develop dedicated medium- and long-term adaptation plans based on the assessment findings. These plans should specify adaptive measures including land-use transitions in high-risk zones and the implementation of managed retreat strategies to complement engineered protection.



**Fig. 3 | Projected exposure of coastal zone functions by scenario combinations, assuming current flood protection standards. a–o,** Exposed functions include population (a–c), ESV (d–f), grain production (g–i), aquaculture production (j–l) and GDP (m–o). In a, d, g, j and m, solid lines show median exposure across three SLR scenarios, with uncertainty bands showing the effects of five policy scenarios. In b, e, h, k and n, solid lines represent

median exposure across three policy scenarios, uncertainty bands showing the effects of three SLR scenarios. In c, f, i, l and o, red bars show decadal variability (range) around SLR scenarios driven by policy; blue bars show decadal variability (range) around policy scenarios driven by SLR. Points represent the range around each of the three scenario combination sets; bar heights indicate the average of the three.

Flood protection is currently the dominant adaptation strategy in China’s coastal zone, but this comes with risks such as the ‘levee effect’—where risk is increased due to development behind levees that are meant to reduce risk—and can be short-sighted, obscuring long-term alternatives such as managed retreat<sup>21</sup>. Our results show as much as a 60% increase in potential impacts to land-system functions when comparing current protection standards to no protection (Supplementary Note 3)—indicating the magnitude of the ‘levee effect’ and the risk posed should protection fail. As of 2017, China has constructed 14,500 km of levees but their completion

times, lifespans and standards vary across regions. Shanghai is the only city with a tide protection standard as high as 1 in 500 years, depending on location, while other parts of the coastline adhere to as low as a 1 in 20-year standard. Furthermore, the construction quality compliance rate is only 42.5% (ref. 22). Our findings reinforce the urgency of improving standards for extreme flood protection and reconsidering the reliance on protection alone for development. In particular, long-term consideration of managed retreat is necessary. The absence of retreat in any of the planning documents we reviewed is concerning and research is required on future adaptation pathways

that include alternatives to protection, such as retreat, accommodation and ecosystem-based adaptation<sup>23</sup>.

Scenario assessments are useful for dealing with future uncertainty and have been widely deployed in climate change contexts. Our analysis contributes to advancing regional and global scenario assessments in three ways: (1) improving existing coastal inundation exposure methodologies; (2) revealing that climate scenarios alone probably underestimate the range of possible futures in terms of coastal flood exposure; and (3) opening the door for the development of detailed adaptation scenarios for coasts (and other areas). Methodologically, DIVA<sup>24,25</sup> has been a leading vector-based framework for regional and global coastal flood risk assessments for over 15 years<sup>4–6,26</sup>. Our high-resolution raster-based framework enables much finer and disaggregated assessments that support spatial planning. Further, our methods can be coupled to other modelling frameworks, including DIVA, to extend the analysis with more detailed spatial adaptation scenarios, such as defend, advance, retreat and accommodate<sup>23</sup>. By adapting the rules in CLUMondo (for example, for spatial constraints), future work using our approach could explore such things as floodplain exclusion zoning or targeted hard protection in different adaptation scenarios.

Our analysis deals with several sources of uncertainty (and agency), including in SLR and its interaction with extreme events; in development policies and their potential to shape different future land systems; in the interactive effects of climate and land-system changes on land subsidence; and in the presence or absence of coastal flood protection measures. Our findings support others that emphasize the importance of considering the range of uncertainty in sets of simulated futures of coastal exposure<sup>27</sup>, as well unpacking what is really driving risk and what can be done to manage it. Our future projections span until 2100. It is imperative to recognize the longer-term risks due to climate change-induced SLR. The Sixth IPCC assessment report (AR6, WG-I) finds that under the highest emissions to 2150, SLR of 2 m is possible and at the high-end 5 m cannot be ruled out. Certainly, SLR continues for centuries and high-end global SLR has been estimated at 2.5 m in 2300 under SSP 1-2.6 and up to 10.4 m in 2300 under SSP 5-8.5 (ref. 28)—why planned retreat must be considered. Importantly, our SLR scenarios omit marine ice sheet and ice cliff instability, which could produce large SLR especially after 2100 under high emissions<sup>29</sup>. General policy responses to such long-term uncertainties are difficult and adaptive policy methods may provide a response framework<sup>30</sup>, which can be supported by our analysis and approach. Ultimately, urgent emissions reductions and prudent adaptive spatial planning are required to reduce risk.

## Online content

Any methods, additional references, Nature Portfolio reporting summaries, source data, extended data, supplementary information, acknowledgements, peer review information; details of author contributions and competing interests; and statements of data and code availability are available at <https://doi.org/10.1038/s41558-025-02439-2>.

## References

1. Adshead, D. et al. Climate threats to coastal infrastructure and sustainable development outcomes. *Nat. Clim. Change* **14**, 344–352 (2024).
2. Hallegatte, S., Green, C., Nicholls, R. J. & Corfee-Morlot, J. Future flood losses in major coastal cities. *Nat. Clim. Change* **3**, 802–806 (2013).
3. Scown, M. W. et al. Global change scenarios in coastal river deltas and their sustainable development implications. *Glob. Environ. Change* **82**, 102736 (2023).
4. Brown, S. et al. Quantifying land and people exposed to sea-level rise with no mitigation and 1.5°C and 2.0°C rise in global temperatures to year 2300. *Earth's Future* **6**, 583–600 (2018).
5. Nicholls, R. J. et al. A global analysis of subsidence, relative sea-level change and coastal flood exposure. *Nat. Clim. Change* **11**, 338–342 (2021).
6. Lincke, D. & Hinkel, J. Economically robust protection against 21st century sea-level rise. *Glob. Environ. Change* **51**, 67–73 (2018).
7. Muis, S. et al. A high-resolution global dataset of extreme sea levels, tides, and storm surges, including future projections. *Front. Mar. Sci.* **7**, 263 (2020).
8. Fang, J. et al. Benefits of subsidence control for coastal flooding in China. *Nat. Commun.* **13**, 6946 (2022).
9. Cortés Arbués, I. et al. Distribution of economic damages due to climate-driven sea-level rise across European regions and sectors. *Sci. Rep.* **14**, 126 (2024).
10. Fang, J. et al. Coastal flood risks in China through the 21st century—an application of DIVA. *Sci. Total Environ.* **704**, 135311 (2020).
11. Wolff, C. et al. A Mediterranean coastal database for assessing the impacts of sea-level rise and associated hazards. *Sci. Data* **5**, 180044 (2018).
12. Cui, Q., Xie, W. & Liu, Y. Effects of sea level rise on economic development and regional disparity in China. *J. Clean. Prod.* **176**, 1245–1253 (2018).
13. Xu, H., Hou, X., Li, D., Zheng, X. & Fan, C. Projections of coastal flooding under different RCP scenarios over the 21st century: a case study of China's coastal zone. *Estuar. Coast. Shelf Sci.* **279**, 108155 (2022).
14. Tebaldi, C. et al. Extreme sea levels at different global warming levels. *Nat. Clim. Change* **11**, 746–751 (2021).
15. Vousdoukas, M. I. et al. Global probabilistic projections of extreme sea levels show intensification of coastal flood hazard. *Nat. Commun.* **9**, 2360 (2018).
16. Pillai, U. P. A. et al. A digital twin modelling framework for the assessment of seagrass nature based solutions against storm surges. *Sci. Total Environ.* **847**, 157603 (2022).
17. Zhang, K. et al. The role of mangroves in attenuating storm surges. *Estuar. Coast. Shelf Sci.* **102–103**, 11–23 (2012).
18. Minderhoud, P. S. J., Middelkoop, H., Erkens, G. & Stouthamer, E. Groundwater extraction may drown mega-delta: projections of extraction-induced subsidence and elevation of the Mekong delta for the 21st century. *Environ. Res. Commun.* **2**, 011005 (2020).
19. Cox, J. R. et al. A global synthesis of the effectiveness of sedimentation-enhancing strategies for river deltas and estuaries. *Glob. Planet. Change* **214**, 103796 (2022).
20. Dunn, F. E. et al. Sedimentation-enhancing strategies for sustainable deltas: an integrated socio-biophysical framework. *One Earth* **6**, 1677–1691 (2023).
21. Hino, M., Field, C. B. & Mach, K. J. Managed retreat as a response to natural hazard risk. *Nat. Clim. Change* **7**, 364–370 (2017).
22. *National Seawall Construction Plan* (NDRC, 2017); [www.ndrc.gov.cn/xxgk/zcfb/tz/201708/W020190905503459462815.pdf](http://www.ndrc.gov.cn/xxgk/zcfb/tz/201708/W020190905503459462815.pdf)
23. Bongarts Lebbe, T. et al. Designing coastal adaptation strategies to tackle sea level rise. *Front. Mar. Sci.* **8**, 740602 (2021).
24. Hinkel, J. & Klein, R. J. T. Integrating knowledge to assess coastal vulnerability to sea-level rise: the development of the DIVA tool. *Glob. Environ. Change* **19**, 384–395 (2009).
25. Vafeidis, A. T. et al. A new global coastal database for impact and vulnerability analysis to sea-level rise. *J. Coast. Res.* **244**, 917–924 (2008).
26. Brown, S. et al. Global costs of protecting against sea-level rise at 1.5 to 4.0°C. *Clim. Change* **167**, 4 (2021).
27. Becker, M., Karpytchev, M. & Hu, A. Increased exposure of coastal cities to sea-level rise due to internal climate variability. *Nat. Clim. Change* **13**, 367–374 (2023).
28. van de Wal, R. S. W. et al. A high-end estimate of sea level rise for practitioners. *Earth's Future* **10**, e2022EF002751 (2022).

29. DeConto, R. M. et al. The Paris Climate Agreement and future sea-level rise from Antarctica. *Nature* **593**, 83–89 (2021).
30. Haasnoot, M., Kwakkel, J. H., Walker, W. E. & ter Maat, J. Dynamic adaptive policy pathways: a method for crafting robust decisions for a deeply uncertain world. *Glob. Environ. Change* **23**, 485–498 (2013).

**Publisher's note** Springer Nature remains neutral with regard to jurisdictional claims in published maps and institutional affiliations.

**Open Access** This article is licensed under a Creative Commons Attribution 4.0 International License, which permits use, sharing,

adaptation, distribution and reproduction in any medium or format, as long as you give appropriate credit to the original author(s) and the source, provide a link to the Creative Commons licence, and indicate if changes were made. The images or other third party material in this article are included in the article's Creative Commons licence, unless indicated otherwise in a credit line to the material. If material is not included in the article's Creative Commons licence and your intended use is not permitted by statutory regulation or exceeds the permitted use, you will need to obtain permission directly from the copyright holder. To view a copy of this licence, visit <http://creativecommons.org/licenses/by/4.0/>.

© The Author(s) 2025

## Methods

We conducted our analysis over the entire coastal zone of mainland China and Hainan. The coastal zone is defined as all coastal prefecture-level cities (spatial administrative areas at the level below province and above county) with 10 km buffer zones along the coastline, covering a land area of 501,300 km<sup>2</sup>.

### Policy review and scenario development

Our previous studies have demonstrated that coastal policies in China play a crucial role in shaping landscape patterns and land use<sup>31–33</sup>, emphasizing the transformative effects of ‘top-down’ policy changes on local landscapes. Thus, here we reviewed coastal zone policies issued from national and provincial authorities that can affect local land-system change<sup>31</sup>.

First, we collected 15 national and 99 provincial coastal zone plans and policies published from 2000 to 2020 (Supplementary Data 1) through extensive searches of government websites and records, which included central and provincial agencies responsible for coastal zones and covered more than two-thirds of prefectural cities along the coastal zone. Along with other attributes, we recorded the orientation of each policy as (1) development-oriented, (2) (ecological) protection-oriented or (3) middle-road orientation or unspecified. Development-oriented policies focus on socioeconomic development, protection-oriented policies focus on ecological protection and middle-road orientation or unspecified balance both objectives and/or have no dominant priority. The classification of policy orientations was based on specific criteria such as policy titles, keyword frequency (for example, protection, development and coordination) and stated policy priorities.

Next, we identified 54 of the 114 documents that contained explicit scenarios beyond 2030. From these, we extracted and analysed their specified (1) planning objectives, (2) spatial strategies and (3) spatial constraints. Planning objectives include value constraints (for example, target values, growth rates and minimum values) and directional semantic descriptions (for example, steady growth, rapid growth and no less than the status quo). Spatial strategies guide the direction and focus of land development (for example, urban expansion, industrial zones and port layouts). Spatial constraints define protected areas such as nature reserves and heritage sites.

From the analysed planning objectives, spatial strategies and spatial constraints, we developed our set of five policy scenarios that are quantitatively characterized by sets of objective parameters (Supplementary Table 1) and spatial rules. These objective parameters and spatial rules were defined by the authors’ expert judgement based on the characteristics of the specific scenarios in the policies analysed and through iterative modelling experiments (Supplementary Note 4). The policy scenarios were broadly defined as ECON, ECOL and MID. The ECON and ECOL scenarios were divided into high and low variants to represent different intensities and stringencies of the policy pathways.

### Projection of land-system changes

We developed a specialized land-system classification for the coastal zone of China, consisting of 21 land-system types at a 1 km<sup>2</sup> resolution and used the CLUMondo model to simulate future land-system changes under different policy scenarios (Supplementary Note 4). Land systems denote mosaic land-use and land-cover patterns caused by a combination of natural and human forces<sup>34</sup>. In the CLUMondo model, land-system changes are driven by regional demand for goods and services and influenced by local driving factors that either promote or constrain land changes<sup>35</sup>. Model inputs include multi-objective parameters, driving factors and spatial rules. Our multi-objective parameters and spatial rules were derived from our policy analysis and scenario development (Supplementary Fig. 7), while the driving factors were selected on the basis of previous research<sup>36,37</sup> and statistical analyses (Supplementary Note 4 and Supplementary Tables 4 and 5).

We selected population, grain production, aquaculture production and ESV as the multi-objective parameters based on the requirements of the CLUMondo model (Supplementary Table 2 and Supplementary Note 4). These values were determined by considering the quantitative policy scenarios (Supplementary Table 1), as well as the development expectations of the coastal zone and its role in the national context.

Spatial constraints include conversion rules, neighbourhood matrix and area restrictions. The conversion rules encompass the difficulty of converting one land system to the others (conversion resistance), whether the conversion from one type to the other is allowed (conversion matrix) and the priority of a land system to be given when allocating for the demand (conversion order). These rules were carefully designed to reflect different policy preferences and trajectories and their details are contained within the model code provided. The matrix of neighbourhood weights (Supplementary Table 3) was calibrated to capture the centripetal forces of urban expansion<sup>35</sup>. The area restrictions indicate areas where land changes are restricted (such as natural reserves) and the special areas allowed for conversion (for example, coastal industry will only appear within a 10-km buffer along the coastline).

### Projection of vertical land-subsidence rates

We developed a 1-km<sup>2</sup> raster map of land subsidence in 2020 for our entire coastal zone using a machine learning model and then projected localized land subsidence under different future scenarios. In our model, future land subsidence is affected by both the policy scenario and the climate scenario. The policy scenario affects land subsidence via different rates depending on the land system in each grid cell, while the climate scenario affects land subsidence via different rates depending on climate variables in the model.

We constructed a dataset of 6,203 sample points of reported subsidence rates, georeferenced from 40 published studies, encompassing major subsidence hotspots along China’s coast (Supplementary Data 2 and Supplementary Note 5). Maps provided in these studies were digitized and subsidence locations along with their respective rates were extracted. The compiled dataset, primarily covering the period 2017–2021, included 4,417 subsidence points (>0 mm yr<sup>-1</sup>) and 1,786 non-subsidence points (0 mm yr<sup>-1</sup>), ensuring a reasonably balanced representation. The sample data represent the most recent and available land-subsidence records.

We used a random forest (RF) regressor to generate maps of localized subsidence. Predictions are made as an ensemble estimate from multiple decision trees based on bootstrap samples (bagging), which helps minimize model overfitting. For model input, we selected 19 explanatory variables representing hydrological, climatic, topographic, geological and anthropogenic factors known to influence subsidence rates<sup>38–40</sup> (Supplementary Table 7). These variables were originally available at different spatial and temporal resolutions, so all of them were resampled to a 1-km<sup>2</sup> resolution and aligned with coastal land areas. Model hyperparameters were optimized through nested cross-validation, using an inner loop for tuning and an outer loop for performance evaluation. Each RF regressor is repeated 20 times using different training and validation samples to evaluate prediction variability and quantify model uncertainty.

Model validation was conducted by comparing predicted and observed subsidence rates at sample points and compared with other recent global studies (Supplementary Note 5). We evaluated the accuracy of the model using mean absolute error (MAE = 3.77 ± 0.268 (mean ± s.d.)) and root mean squared error (RMSE = 7.525 ± 1.124) and coefficient of determination ( $R^2 = 0.6 \pm 0.08$ ), which are acceptable given observed subsidence rates as high as 240 mm yr<sup>-1</sup>.

Finally, projection of future land subsidence under the various scenario combinations was done by replacing the current land system and climate explanatory variables with their future projections in each

1-km<sup>2</sup> grid cell. The land-system type was taken from the projected land-system maps under each policy scenario. The most influential land system on land subsidence in our best-performing RF model was coastal industry, followed by urban, suburban and inland industry (Supplementary Fig. 15). The four most influential bioclimatic variables from the best-performing RF model were precipitation seasonality, precipitation in the wettest quarter, temperature diurnal range and mean annual temperature (Supplementary Figs. 15 and 16); these were replaced with projected values from the MRI-ESM2-0 model<sup>41</sup>. Because these climate data are available in 20-yr intervals, we used the RF model to produce maps of annual land-subsidence rate (in mm) for 2030, 2050, 2070 and 2090. The annual subsidence rate (mm) for each 1-km<sup>2</sup> pixel was accumulated yearly using the initial rate of each period: the rate of 2020 for 2020–2029, then adding the rate of 2030 for 2030–2049, the rate of 2050 for 2050–2069 and so on. We assumed that the relationships among features in the RF model remain constant over time.

### Projections of extreme relative sea levels

Our analysis includes the important components of mean SLR, land subsidence and transient extreme events due to high tides and storm surges corresponding to the 1 in 100 return period. This approach was selected from a maximum-risk management perspective—that is, reflecting the maximum risk from extreme events with potential for extensive impacts. From a policy-maker's perspective, it is often useful to adopt a cautious approach and prepare for the worst-case scenario, even if the probabilities are low<sup>42</sup>.

To integrate long-term SLR with short-term extreme events, we express the future ESL (or extreme coastal water level) in year  $t$  as a linear combination, as shown in equation (1):

$$ESL_t = MSL + SLR_t + TS + CCE_{x_{int}} \quad (1)$$

where MSL is mean sea level, specified by the vertical datum of the data used.  $SLR_t$  is the amount of SLR in year  $t$ , excluding relative land motion. The values of tides and storm surges (TS) are extremes obtained for a specific return period based on historical records.  $CCE_{x_{int}}$  is a factor capturing the interactive effect between climate change and extreme events.

We calculated the ESL projections in different SLR scenarios up to 2100. The SLR projections are derived from IPCC AR6 data<sup>43</sup>, incorporating various components of future SLR, such as steric SLR, dynamic sea-level change, contributions from glaciers and ice caps and land-water storage. To avoid double-counting land-subsidence effects, we use values of the novlm (no vertical land motion) version with median confidence. We took three scenarios from the AR6 data: SSP 1-2.6 (5th percentile from the model ensemble; low-end), SSP 2-4.5 (median from the model ensemble; mid-range) and SSP 5-8.5 (95th percentile from the model ensemble; high-end). We chose the 5th and 95th percentiles of the low- and high-end scenarios, respectively, to cover the wide range of possible futures. While SLR differences are primarily associated with RCP (climate) differences, SSPs can, for example, alter land-water storage effects. Importantly, we do not include key features of potential SLR, such as marine ice cliff instability and marine ice sheet instability. These factors could substantially modulate the potential end-of-century SLR outcomes, but they are not well understood and are considered low confidence in AR6.

Climate change not only affects SLR, but also extreme events and understanding these effects presents substantial challenges. Previous studies<sup>44</sup> have revealed seemingly contradictory effects: extreme events can either amplify with SLR as a result of decreased bottom friction effects, or diminish because of reduced surface wind stress or deeper water columns. Such complexity underscores that the SLR–extreme event interaction is not simply additive but involves complex hydrodynamic interactions that can produce counterintuitive outcomes, strongly modulated by local characteristics such as

coastal geometry, bathymetry, tidal regime and freshwater inputs<sup>45</sup>. Notably, the response of tidal constituents—such as mean high water and tidal range—is often disproportionate to the magnitude of SLR. In many locations, mean high water exhibits a super-proportional response, suggesting an amplifying effect of tidal dynamics under higher sea levels<sup>46</sup>. For instance, in China's Pearl River Delta, tidal amplification may exceed 0.5 m under a projected SLR of 2.1 m, primarily due to depth-induced reductions in bottom friction<sup>44</sup>. A European analysis spanning 1960 to 2018 found that trends in surge extremes closely tracked mean sea-level changes, influenced by both internal climate variability and anthropogenic forcing<sup>47</sup>. Global analyses have found that the effect of climate change on extreme sea levels is mostly driven by SLR and an interactive effect of SLR with TS<sup>7,15</sup>. While increased intensity storms can have a relatively large contribution to extreme events in some areas, their interactive effect with SLR can be reversed in others, leading to minimal regional contributions of storm surges (see Fig. 6 in ref. 15). In the Yangtze River Estuary, for example, SLR could lead to a 1-m increase in water depth, which in turn may reduce the maximum storm surge by approximately 0.15 m (ref. 48).

Given the complexities in the climate change–extreme event interaction, we conducted multiple analyses to capture uncertainty. First, we calculated our future extreme sea levels with the  $CCE_{x_{int}}$  factor set to zero. Next, we assessed the effects of increasing this factor incrementally as 10% and 30% of SLR in each cell—more than covering the maximum 25% found in the Chinese case studies we examined<sup>44</sup>. The main text contains the water depth results for  $CCE_{x_{int}} = 0.1$  SLR (Fig. 2) while water depth results for  $CCE_{x_{int}} = 0$  and  $CCE_{x_{int}} = 0.3$  SLR can be found in Supplementary Note 2. All combinations of these scenarios are captured in the variability analyses in Fig. 3. Note that we do not analyse a potential overall reduction in ESL through this interaction term, which would lower the exposure caused by SLR scenarios.

The land elevation data were defined by CoastalDEM<sup>49</sup>, whose vertical datum is the EGM96 geoid. The TS data were sourced from the coastal dataset for the evaluation of climate impact (CoDEC) dataset<sup>7</sup>. To convert the vertical datum of the CoDEC extremes from MSL to EGM96, we referred to previous studies<sup>50</sup> and used the mean dynamic ocean topography (MDT) CNES-CLS22 data for conversion<sup>51</sup>. Localized land subsidence was taken from the RF model.

### Coastal flood exposure

Coastal flood exposure assessments are often conducted using a simple bathtub model, which overestimates inundated area by not accounting for hydrodynamics<sup>52</sup>. We used an improved geometric inundation model that considers hydrological connectivity and attenuation to project coastal flood exposure caused by SLR, land subsidence and extreme sea levels. The modelling process begins at pixels that represent the current land–ocean border and iteratively spreads inward (Supplementary Note 6). Ocean water propagates from current oceans and inundates neighbouring cells whose elevation is below a specific value subtracting the attenuation coefficient from ESL, with iterations until no cells can be inundated. It aims to minimize the overestimation of unrealistic inundation extents or depths compared with a conventional bathtub model<sup>53</sup>.

The water depth  $W_{t,i}$  of the inundated pixel  $i$  at year  $t$  is computed using equation (2):

$$W_{t,i} = \begin{cases} (ESL_{t,i} - H_{t,i} - a_{t,i}) \times \mathcal{C}_{t,i}, & SL_{t,i} > H_{t,i} + a_{t,i} \\ 0, & ESL_{t,i} \leq H_{t,i} + a_{t,i} \end{cases} \quad (2)$$

where:

- $ESL_{t,i}$  is the projected ESL for pixel  $i$  at year  $t$ ;
- $H_{t,i}$  refers to the difference between the original elevation and the projected land subsidence for pixel  $i$  at year  $t$ ;

- $\alpha_{t,i}$  denotes attenuation, accounting for the diminishing impact of water as it moves inland from the coastal starting point to pixel  $i$  at year  $t$  (see Supplementary Note 6 for sensitivity analysis);
- $\mathcal{C}_{t,i}$  is a binary parameter, representing whether the pixel  $i$  is connected to water (=1) or not (=0) at year  $t$ , using the cardinal and diagonal connectivity rule.

To perform a localized assessment of the projected ESL values along the land–ocean border, we first extracted a high-resolution ocean mask using CoastalDEM and our land cover classification products (Supplementary Note 6), which includes fully interconnected river mouths. The spatial resolution of the CoastalDEM was resampled from 90 m to 100 m to align with the land system’s resolution of 1,000 m. We used the inverse distance weighting (IDW) interpolation algorithm to downscale various datasets to a 100-m resolution, thereby matching the resolution needed for localized projections. The datasets include  $1^\circ \times 1^\circ$  IPCC SLR data and  $0.25^\circ \times 0.25^\circ$  MDT data in raster format, as well as 100-return period CoDEC data in point format. The raster data were converted to points using Raster to Point function in ArcGIS. The CoDEC points were used as control points in the IDW interpolation to create a 100-m resolution SLR map for each component. The spatial mask and raster to be snapped were set as the derived ocean mask. Finally, we used the Plus function in ArcGIS to sum the values on a cell-by-cell basis.

We compared results for all subsequent analyses using both a simple bathtub model (attenuation factor = 0) and our improved geometric inundation model (attenuation factor > 0) on the basis of inspection of inundation maps across a range of attenuation factors (Supplementary Fig. 21). Our findings presented in the main text use an attenuation factor = 0.01 and are consistent with the rank-order results from the simple bathtub model (Supplementary Fig. 22), although absolute values differ.

We adjusted inundation exposure extents based on current coastal protection standards along the Chinese coast. These standards vary considerably by city and county, from  $\geq 200$ -yr return period in major cities to <50-yr return period along most of the coastline (and as low as 20-yr return period in some very vulnerable parts). We used the flood protection level map from ref. 54 to overlay protection standards (in return period) for cities and counties throughout our coastal zone. Since our water depth calculations used the 1 in 100-yr extreme event, we assumed grid cells are inundated wherever protection standards are less than the 100-yr return period. Wherever protection standards were  $\geq 100$ -yr return period, we assumed complete and successful implementation of the protection standards and, therefore, no inundation. This is probably an overestimate of real protection levels, since standards are not always met in reality, so we also conducted the full analysis assuming no protection, which gives us the best and worst cases in terms of coastal protection.

### Potential impact evaluation

We analysed the potential impacts associated with inundation assuming current coastal protection standards are met, as well as assuming no protection. The functions supported by different land systems include human habitation (population), GDP, grain production, aquaculture and ESV. Population, grain and aquaculture production and ESV were calculated for each pixel directly from CLUMondo. GDP was estimated from the land-system map for each policy scenario each year. First, the average GDP per pixel of each land-system type in 2020 was calculated from the 2020 land-system map and a downscaled 2020 GDP grid. Then, for each scenario, the number of inundated pixels of each land-system type was calculated and multiplied by the average per pixel GDP for that land-system type. This accounts for future changes in GDP based on our land-system changes, but it does not account for future GDP growth, currency decline, nor discount rates. Thus, our absolute values

of GDP and ESV exposure should be considered underestimates for the future. However, the absolute values of these metrics are not of primary concern when considering the relative effects of SLR scenarios versus policy scenarios, as we do here, since any growth and discounting functions would have the same relative effect on the metrics under both sets of scenarios.

To quantify and categorize different levels of potential SLR impacts, we classified inundation depths on the basis of their distribution characteristics into five categories: 0–1 m, 1–2 m, 2–3.5 m, 3.5–5 m and 5 m or more. To comprehensively assess exposure across different scenarios, we overlaid land-system data with coastal flooding projections at a spatial resolution of 1 km<sup>2</sup>. This analysis was conducted across the full range of policy and SLR scenario combinations over time.

To compare the magnitude of variation in exposure between policy and SLR scenarios, we calculated the exposure of different functions for each policy scenario overlaid with the inundation ranges of each SLR scenario, as well as the exposure for each SLR scenario overlaid with each policy scenario. For instance, to assess the range of variation in exposure due to SLR scenarios under the middle-road policy, we overlaid the land-system map of the middle-road scenario with inundation maps representing low-end, mid-range and high-end SLR scenarios for each year. We then calculated the multifunctional exposure. The range of variation was determined by the difference between the maximum and minimum values of these three observations, representing the exposure variation attributable solely to changes in SLR scenarios within the middle-road policy scenario, for that year. The same approach was applied to the other four policy scenarios to obtain a complete range of variation due to SLR scenarios. Similarly, the variation attributable to policy scenarios was calculated by sequentially combining the same SLR scenario with different policy scenarios. In this way, we could identify whether SLR or policy scenarios had the largest effect on exposure for each land-system function.

### Reporting summary

Further information on research design is available in the Nature Portfolio Reporting Summary linked to this article.

### Data availability

The projected land-system maps for five policy scenarios, together with associated validation datasets and sampling points for projecting land subsidence, are available via figshare at <https://doi.org/10.6084/m9.figshare.29263130> (ref. 55). The input data used in CLUMondo for land-system change simulations are cited throughout the paper, with full details provided in Supplementary Note 4 and Supplementary Table 4. The SLR data were obtained from the IPCC AR6 database, available via Zenodo at <https://doi.org/10.5281/zenodo.6382554> (ref. 43), while tide and surge data were sourced from the CoDEC dataset, available via Zenodo at <https://doi.org/10.5281/zenodo.3660927> (ref. 56). The CoastalDEM were acquired from Climate Central (<https://go.climatecentral.org>) and MDT data were obtained from AVISO (<https://doi.org/10.24400/527896/a01-2023.003>). Sources for explanatory factors used in predicting land-subsidence rates are listed in Supplementary Table 7. All data supporting this study are provided with the paper.

### Code availability

The CLUMondo model is publicly available via GitHub at <https://github.com/VUEG/CLUMondo>. Python scripts used for projecting land subsidence and generating figures can be accessed via figshare at <https://doi.org/10.6084/m9.figshare.29263130> (ref. 55). The improved geometric inundation model, which incorporates hydrological connectivity and attenuation, is available via GitHub at [https://github.com/geoye/attenuated\\_bathtub](https://github.com/geoye/attenuated_bathtub). Additional code supporting the findings of this study is available from the corresponding authors upon reasonable request.

## References

31. Wang, Y., Liao, J., Ye, Y., O'Byrne, D. & Scown, M. W. Implications of policy changes for coastal landscape patterns and sustainability in Eastern China. *Landsc. Ecol.* **39**, 4 (2024).
32. Wang, Y., Liao, J., Ye, Y. & Fan, J. Long-term human expansion and the environmental impacts on the coastal zone of China. *Front. Mar. Sci.* **9**, 1033466 (2022).
33. Fan, J. et al. Reshaping the sustainable geographical pattern: a major function zoning model and its applications in China. *Earth's Future* **7**, 25–42 (2019).
34. Van Asselen, S. & Verburg, P. H. A Land System representation for global assessments and land-use modeling. *Glob. Change Biol.* **18**, 3125–3148 (2012).
35. van Asselen, S. & Verburg, P. H. Land cover change or land-use intensification: simulating land system change with a global-scale land change model. *Glob. Change Biol.* **19**, 3648–3667 (2013).
36. Kim, Y., Newman, G. & Güneralp, B. A review of driving factors, scenarios, and topics in urban land change models. *Land* **9**, 246 (2020).
37. Wang, Y., van Vliet, J., Debonne, N., Pu, L. & Verburg, P. H. Settlement changes after peak population: land system projections for China until 2050. *Landsc. Urban Plan.* **209**, 104045 (2021).
38. Davydenko, T., Tahmasebi, P. & Shokri, N. Unveiling the global extent of land subsidence: the sinking crisis. *Geophys. Res. Lett.* **51**, e2023GL104497 (2024).
39. Hasan, M. F., Smith, R., Vajedian, S., Pommerenke, R. & Majumdar, S. Global land subsidence mapping reveals widespread loss of aquifer storage capacity. *Nat. Commun.* **14**, 6180 (2023).
40. Herrera-García, G. et al. Mapping the global threat of land subsidence. *Science* **371**, 34–36 (2021).
41. Yukimoto, S. et al. The Meteorological Research Institute Earth System Model Version 2.0, MRI-ESM2.0: description and basic evaluation of the physical component. *J. Meteorol. Soc. Jpn II* **97**, 931–965 (2019).
42. Bachner, G., Lincke, D. & Hinkel, J. The macroeconomic effects of adapting to high-end sea-level rise via protection and migration. *Nat. Commun.* **13**, 5705 (2022).
43. Garner, G. G. et al. IPCC AR6 sea level projections (version 20210809). *Zenodo* <https://doi.org/10.5281/zenodo.6382554> (2021).
44. De Dominicis, M., Wolf, J., Jevrejeva, S., Zheng, P. & Hu, Z. Future interactions between sea level rise, tides, and storm surges in the world's largest urban area. *Geophys. Res. Lett.* **47**, e2020GL087002 (2020).
45. Khojasteh, D., Chen, S., Felder, S., Heimhuber, V. & Glamore, W. Estuarine tidal range dynamics under rising sea levels. *PLoS ONE* **16**, e0257538 (2021).
46. Pickering, M. D. et al. The impact of future sea-level rise on the global tides. *Cont. Shelf Res.* **142**, 50–68 (2017).
47. Calafat, F. M., Wahl, T., Tadesse, M. G. & Sparrow, S. N. Trends in Europe storm surge extremes match the rate of sea-level rise. *Nature* **603**, 841–845 (2022).
48. Shen, Y., Deng, G., Xu, Z. & Tang, J. Effects of sea level rise on storm surge and waves within the Yangtze River Estuary. *Front. Earth Sci.* **13**, 303–316 (2019).
49. Kulp, S. A. & Strauss, B. H. New elevation data triple estimates of global vulnerability to sea-level rise and coastal flooding. *Nat. Commun.* **10**, 4844 (2019).
50. Muis, S. et al. A comparison of two global datasets of extreme sea levels and resulting flood exposure. *Earth's Future* **5**, 379–392 (2017).
51. Jousset, S. et al. *New Global Mean Dynamic Topography CNES-CLS-22 Combining Drifters, Hydrological Profiles and High Frequency Radar Data* (OSTST, 2022); <https://doi.org/10.24400/527896/A03-2022.3292>
52. Sanders, B. F., Wing, O. E. J. & Bates, P. D. Flooding is not like filling a bath. *Earth's Future* **12**, e2024EF005164 (2024).
53. Kasmalkar I. Flow-tub model: a modified bathtub flood model with hydraulic connectivity and path-based attenuation. *MethodsX* **12**, 102524 (2024).
54. Wang, D., Scussolini, P. & Du, S. Assessing Chinese flood protection and its social divergence. *Nat. Hazards Earth Syst. Sci.* **21**, 743–755 (2021).
55. Wang, Y. et al. Development policy affects coastal flood exposure in China more than sea-level rise. *figshare* <https://doi.org/10.6084/m9.figshare.29263130> (2025).
56. Muis, S. et al. CoDEC Dataset—data underlying the paper “A high-resolution global dataset of extreme sea levels, tides and storm surges including future projections”. *Zenodo* <https://doi.org/10.5281/zenodo.3660927> (2020).

## Acknowledgements

This research was funded by the National Natural Science Foundation of China (grant nos 42371184, 42001131 and W2421009). We thank the China Scholarship Council and the CAS President's International Fellowship Initiative for their financial support. We thank J. Liao, Z. Shen, S. Shen and Y. Fan for their contributions to data and policy document collection and visualizations.

## Author contributions

Y.W. and M.S. conceptualized the study. Y.W., Y.Y., M.L. and J.F. developed the policy scenario and land systems methodology. Y.W., Y.Y., M.S. and R.J.N. developed the relative SLR and exposure methodology. Y.W. designed the scenarios. Y.W., Y.Y. and Y.H. curated the data, ran the models and performed the data analysis. Y.W., Y.Y. and M.S. carried out the investigation. Y.W. and M.S. wrote the original draft. M.S., Y.W., Y.Y., R.J.N., L.O., D.P.v.V., G.P., M.L. and J.F. discussed the results and contributed to the review and editing of the paper. Y.W., Y.Y. and M.S. created the visualizations. Y.W. acquired the funding.

## Funding

Open access funding provided by Lund University.

## Competing interests

The authors declare no competing interests.

## Additional information

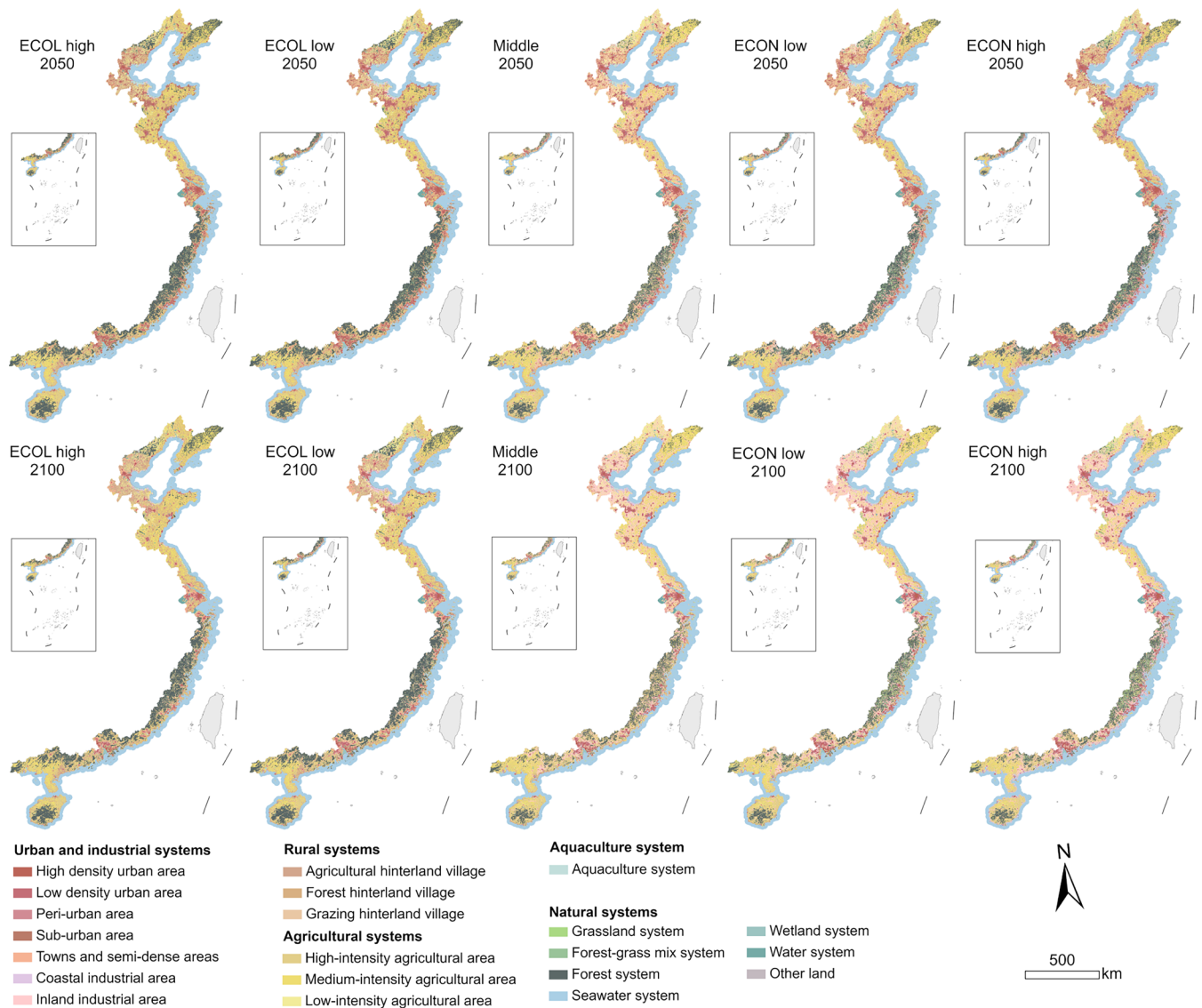
**Extended data** is available for this paper at <https://doi.org/10.1038/s41558-025-02439-2>.

**Supplementary information** The online version contains supplementary material available at <https://doi.org/10.1038/s41558-025-02439-2>.

**Correspondence and requests for materials** should be addressed to Yafei Wang or Murray Scown.

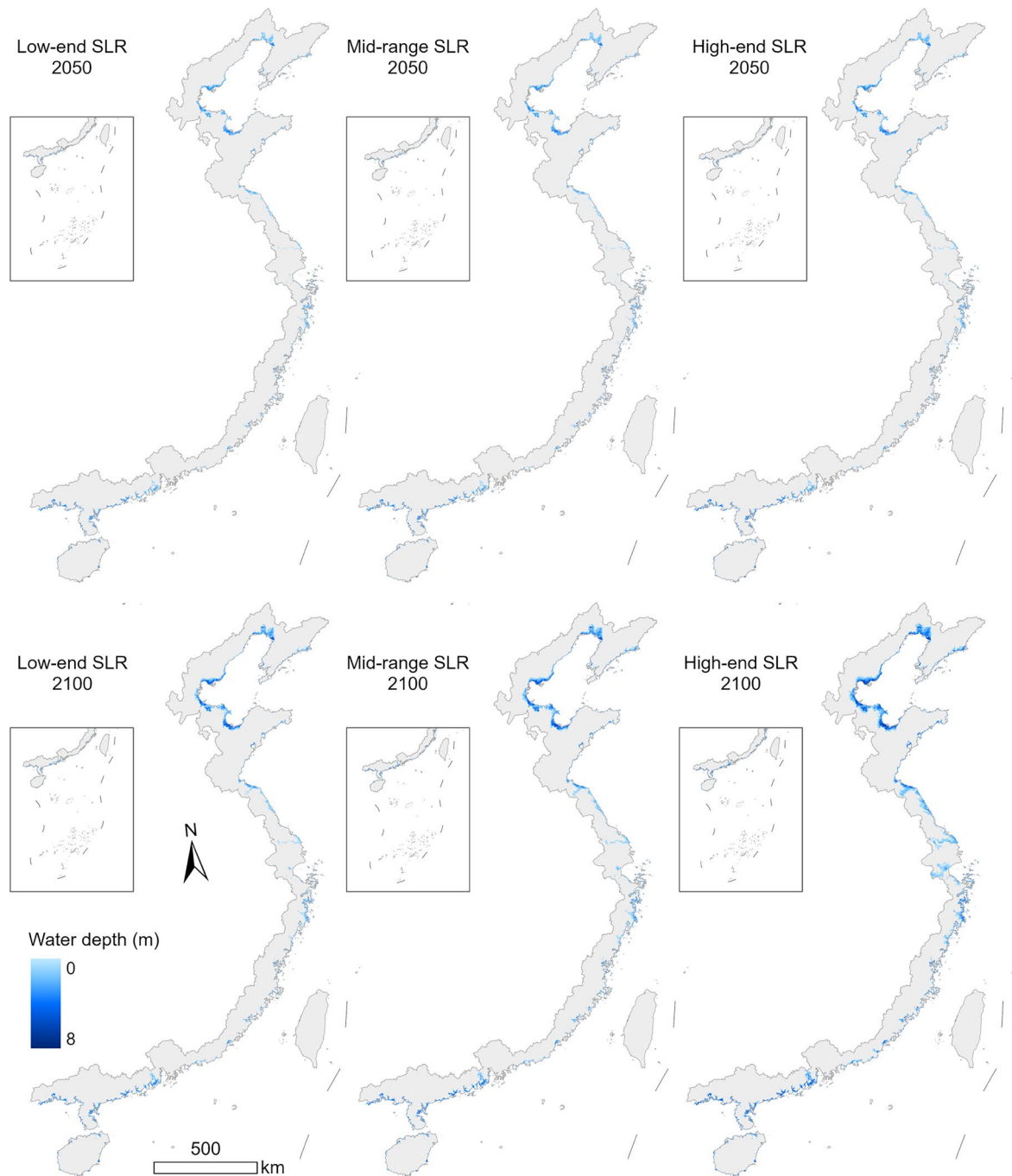
**Peer review information** *Nature Climate Change* thanks Yi Fan and the other, anonymous, reviewer(s) for their contribution to the peer review of this work.

**Reprints and permissions information** is available at [www.nature.com/reprints](http://www.nature.com/reprints).



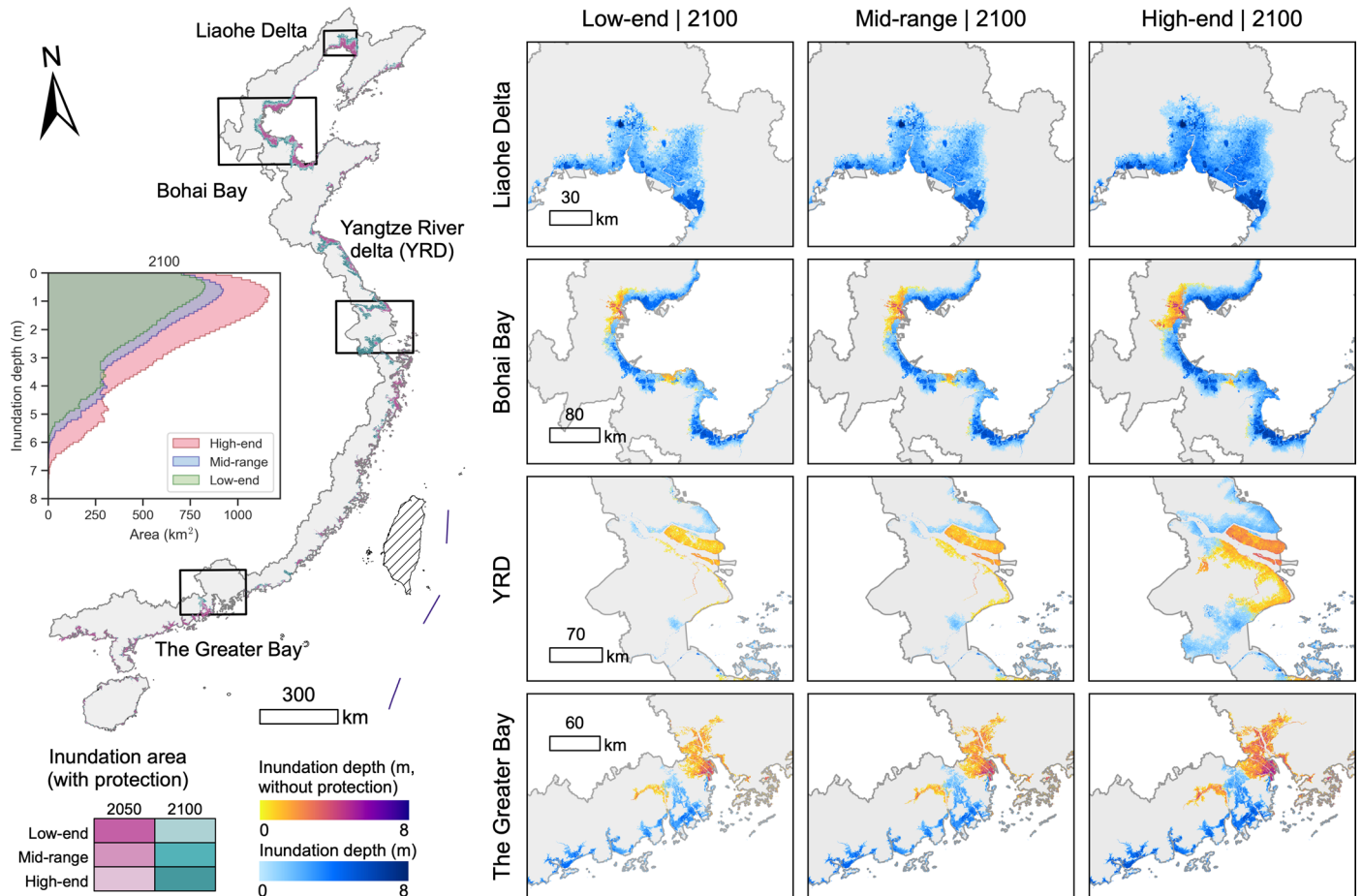
**Extended Data Fig. 1 | National land system projections under different policy scenarios in 2050 and 2100.** The policy scenarios were broadly categorized as economic development-oriented ('ECON'), ecological protection-oriented ('ECOL'), and a middle-ground pathway ('Middle road'). Both ECON and ECOL scenarios include high and low variants to represent different levels of policy

intensity and stringency. The projections include five major groups—urban and industrial systems, rural systems, agricultural systems, aquaculture systems, and natural systems—comprising 21 land system types at a 1 km<sup>2</sup> resolution. Maps created with ArcGIS Pro 3.4. Basemap data from the National Catalogue Service for Geographic Information (<https://www.webmap.cn>).



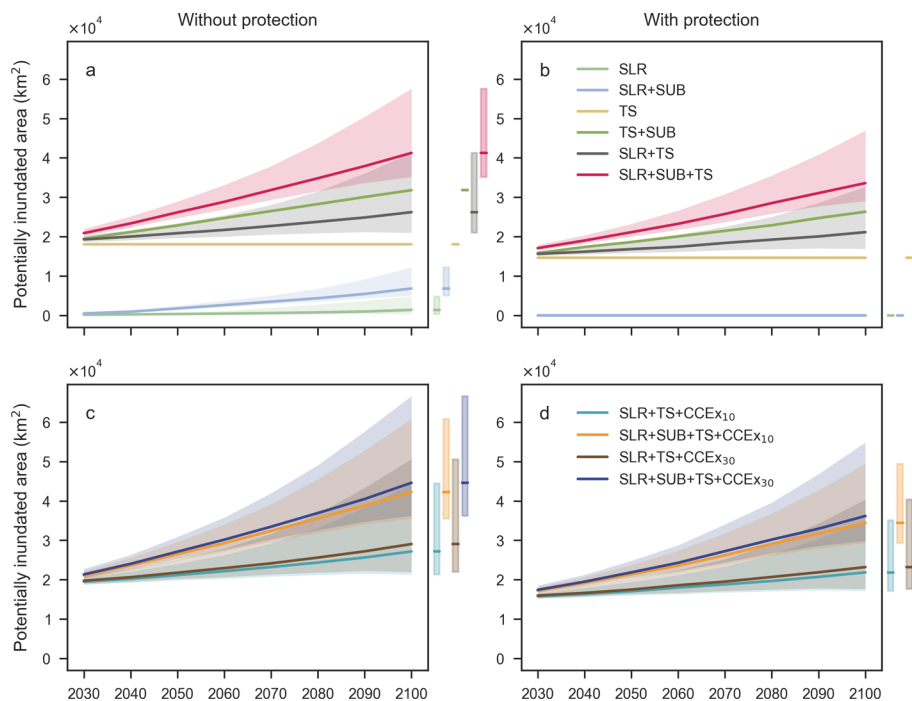
**Extended Data Fig. 2 | The inundation results for three sea-level rise (SLR) scenarios in 2050 and 2100 in China's coastal zone.** Simulations assume an attenuation factor of 0.01 m/pixel (100 m), current protection standards, and a 10% interactive effect between SLR and extreme events. We used three SLR scenarios from the AR6 model ensemble to represent a wide range of possible

future scenarios: a low-end scenario (SSP1-2.6, 5th percentile), a mid-range scenario (SSP2-4.5, ensemble median), and a high-end scenario (SSP5-8.5, 95th percentile). The 5th and 95th percentiles were selected to capture lower- and upper-bound estimates of projected SLR. Maps created with ArcGIS Pro 3.4. Basemap data from the National Catalogue Service for Geographic Information (<https://www.webmap.cn>).



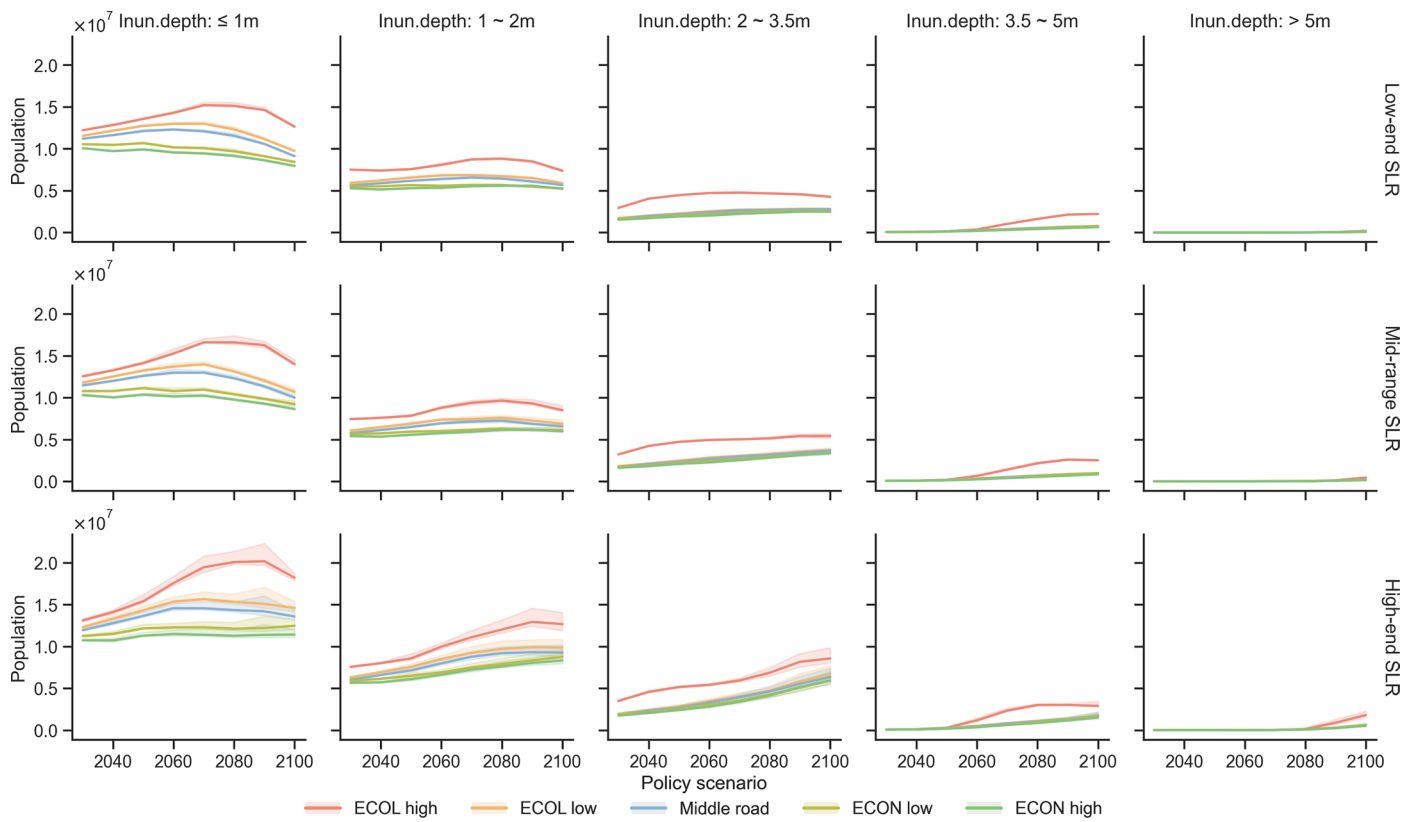
**Extended Data Fig. 3 | Projections exposure of four delta regions to coastal flooding under different scenarios, with and without current protection standards and a 10% inactive effect between sea-level rise (SLR) and extreme events.** The main map depicts the overview spatial pattern of areas potentially exposed to flooding under three SLR scenarios for 2050 and 2100. The inset on the left represents the distribution of water depths under three SLR scenarios in 2100 with current protection standards. The regional zooms show the inundation

depth patterns in the four key delta regions, with inundation depth assuming current protection standards shown in blue, as well as potential inundation assuming no protection (that is, if protection fails) shown in yellow to purple. The blue areas potentially inundated with current protection standards are the same when assuming no protection (that is, they are inundated either way). Maps created with ArcGIS Pro 3.4. Basemap data from the National Catalogue Service for Geographic Information (<https://www.webmap.cn>).



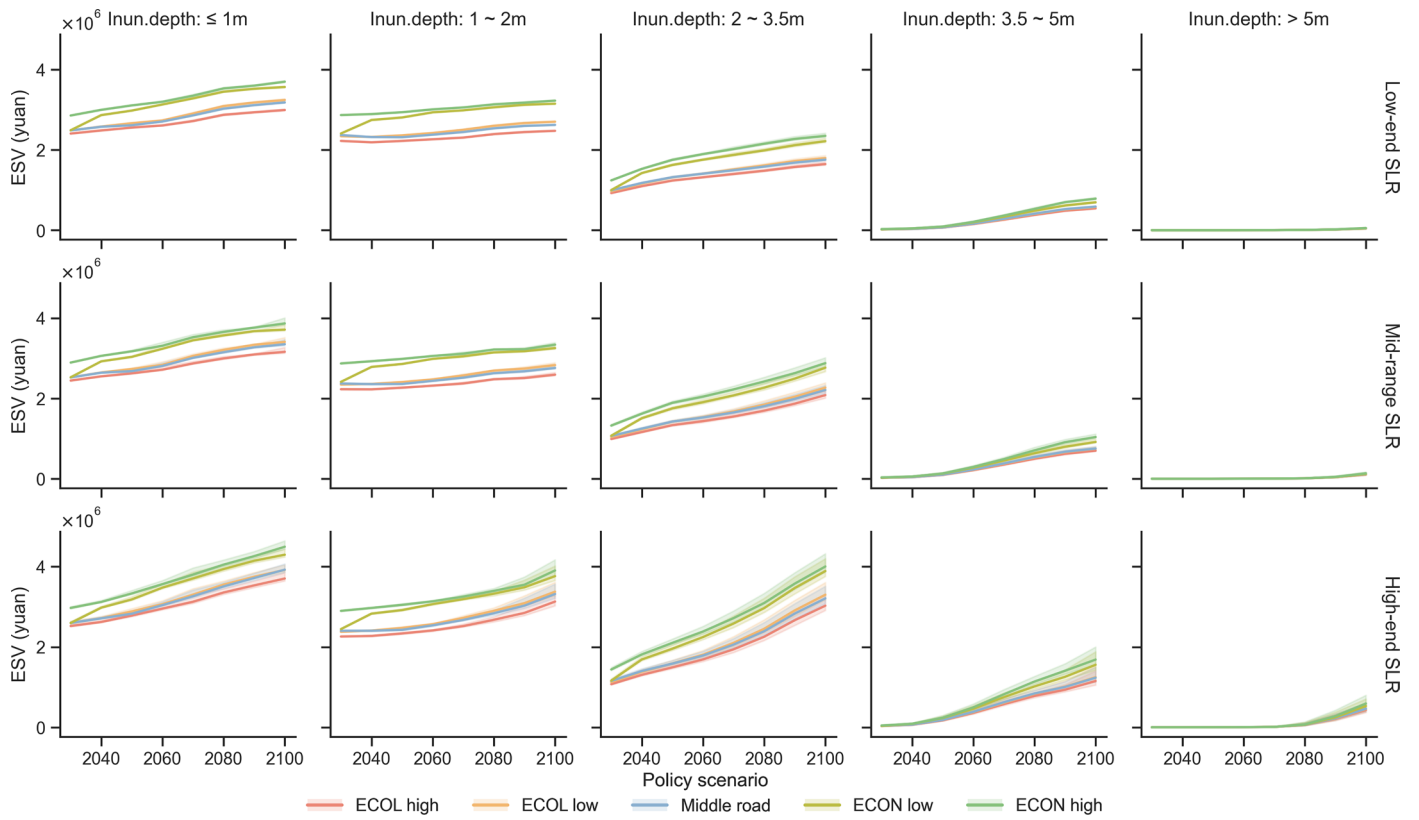
**Extended Data Fig. 4 | Contribution of different relative sea level components to flood exposure extent with different assumptions.** Left panels (a, c) show potential inundation area without protection, and right panels (b, d) show the same with current protection standards. Top panels (a, b) show the disaggregated effects of sea-level rise (SLR), land subsidence, and tides and storms, and bottom panels (c, d) show the added effects of interactions between SLR and extreme events at values of 10% and 30% of SLR. The coastal area potentially inundated when considering different combinations of components is shown at ten-year intervals from 2030 to 2100, using an attenuation factor of 0.01 m/pixel (100 m). Mean SLR and the rate of land subsidence (SUB) varies temporally and spatially based on differences in scenarios; while tides and

storm surges (TS) vary spatially but remain constant over time and equal across scenarios. CCE<sub>x10</sub> and CCE<sub>x30</sub> indicate, respectively, a 10% and 30% inactive effect between SLR and extreme events, compared to panels (a) and (b), which have essentially a 0% interactive effect. The uncertainty band represents the range of inundated area across different SLR scenarios (see methods for full details). The solid lines on the main plot represent the mid-range SLR scenario (or TS when SLR is not added), and the uncertainty bands show the range of potentially inundated area among all scenario combinations. The shaded bars on the right show the range of area in 2100, and the horizontal lines represent the mid-range SLR scenario (or TS when SLR is not added).

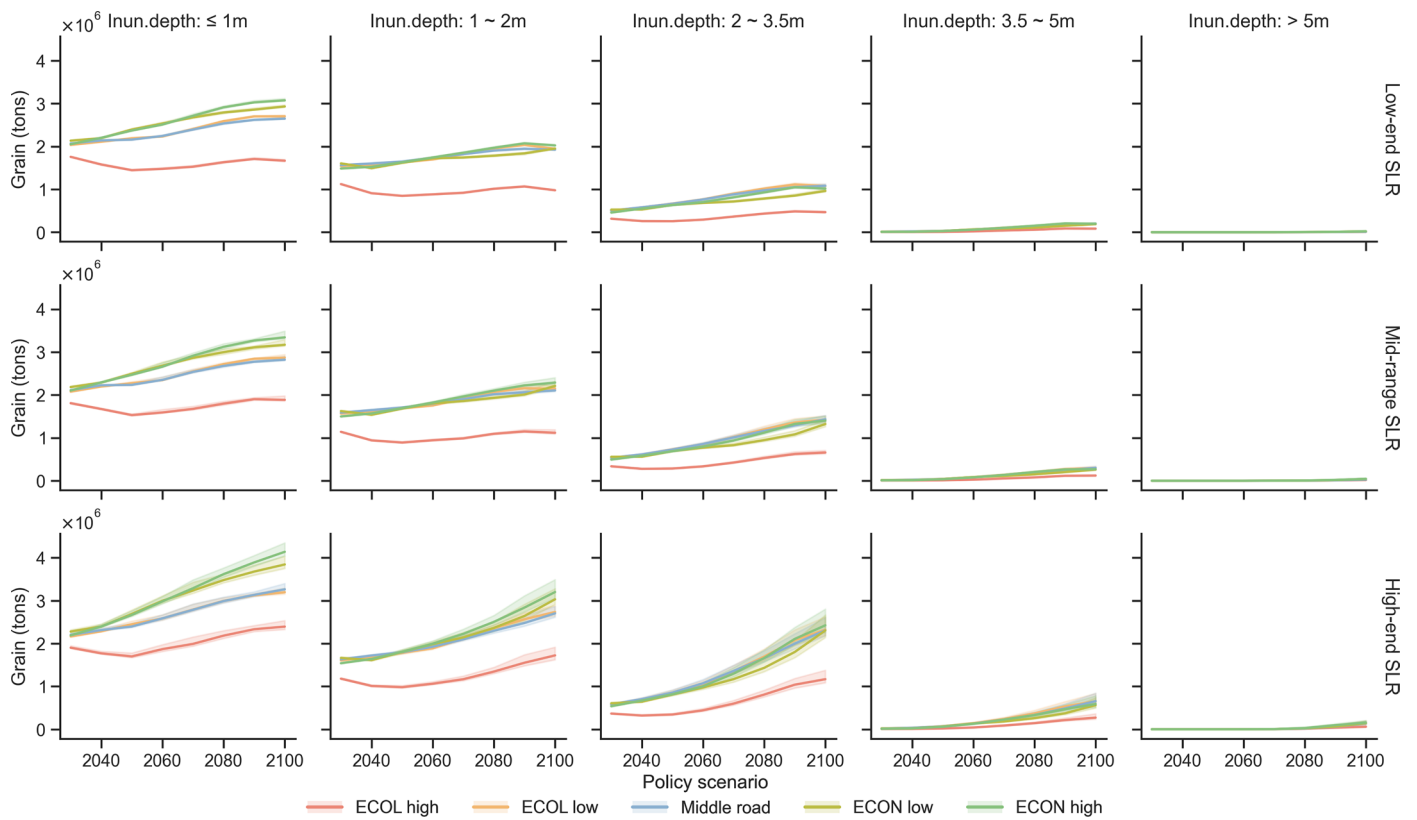


**Extended Data Fig. 5 | Comparison of exposed population by inundation depth under different scenarios with current flood protection standards.** Solid lines represent the exposure values for  $CCE_{x_{10}}$ , and shaded bands indicate

the upper and lower bounds of  $CCE_{x_{30}}$  and sea-level rise (SLR) scenario with no interaction.  $CCE_{x_{10}}$  and  $CCE_{x_{30}}$  indicate, respectively, a 10% and 30% inactive effect between SLR and extreme events.

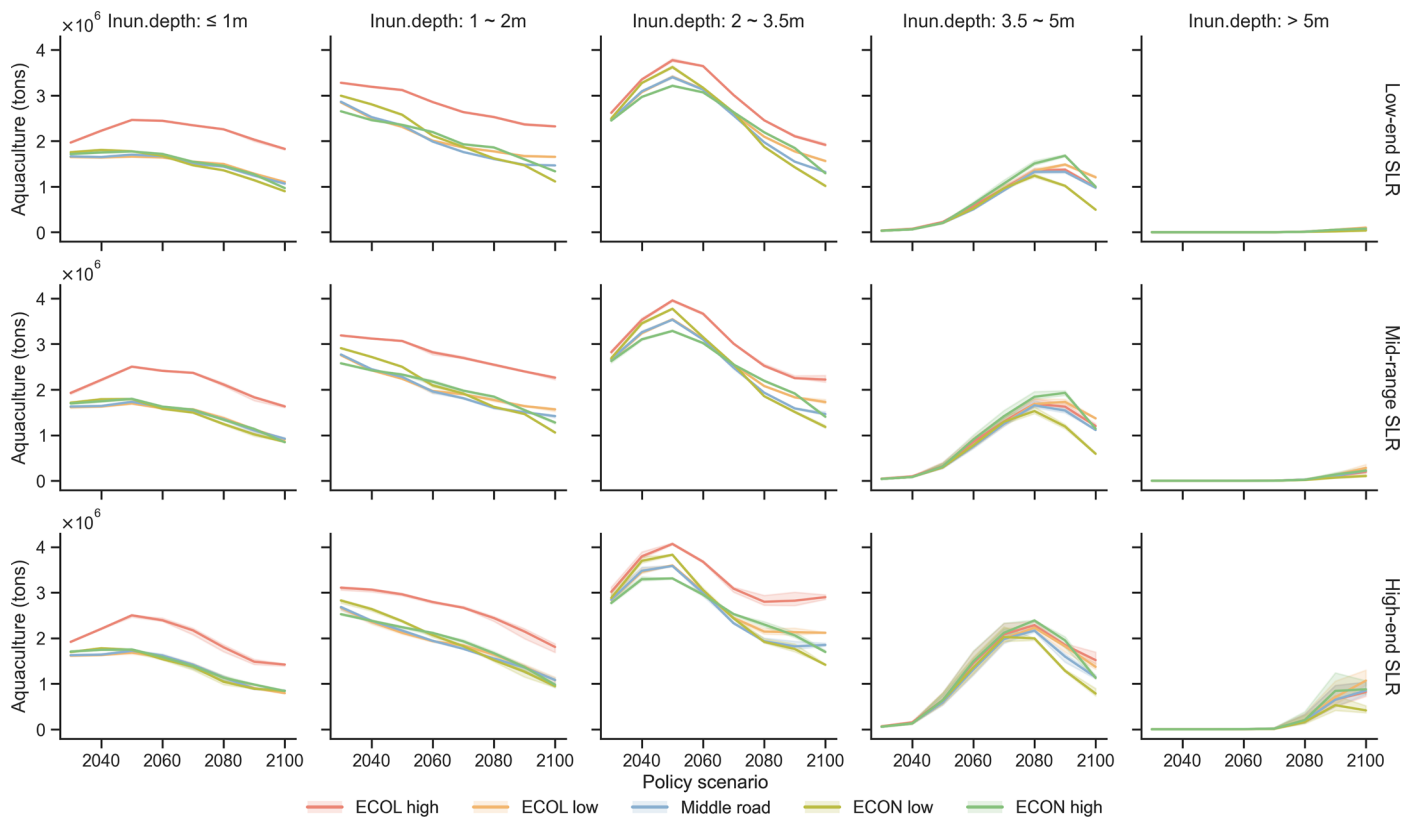


**Extended Data Fig. 6 | Comparison of exposed GDP by inundation depth under different scenarios with current flood protection standards.** Solid lines represent the exposure values for  $CCEx_{10}$ , and shaded bands indicate the upper and lower bounds of  $CCEx_{30}$ , and sea-level rise (SLR) scenario with no interaction.  $CCEx_{10}$  and  $CCEx_{30}$  indicate, respectively, a 10% and 30% inactive effect between SLR and extreme events.



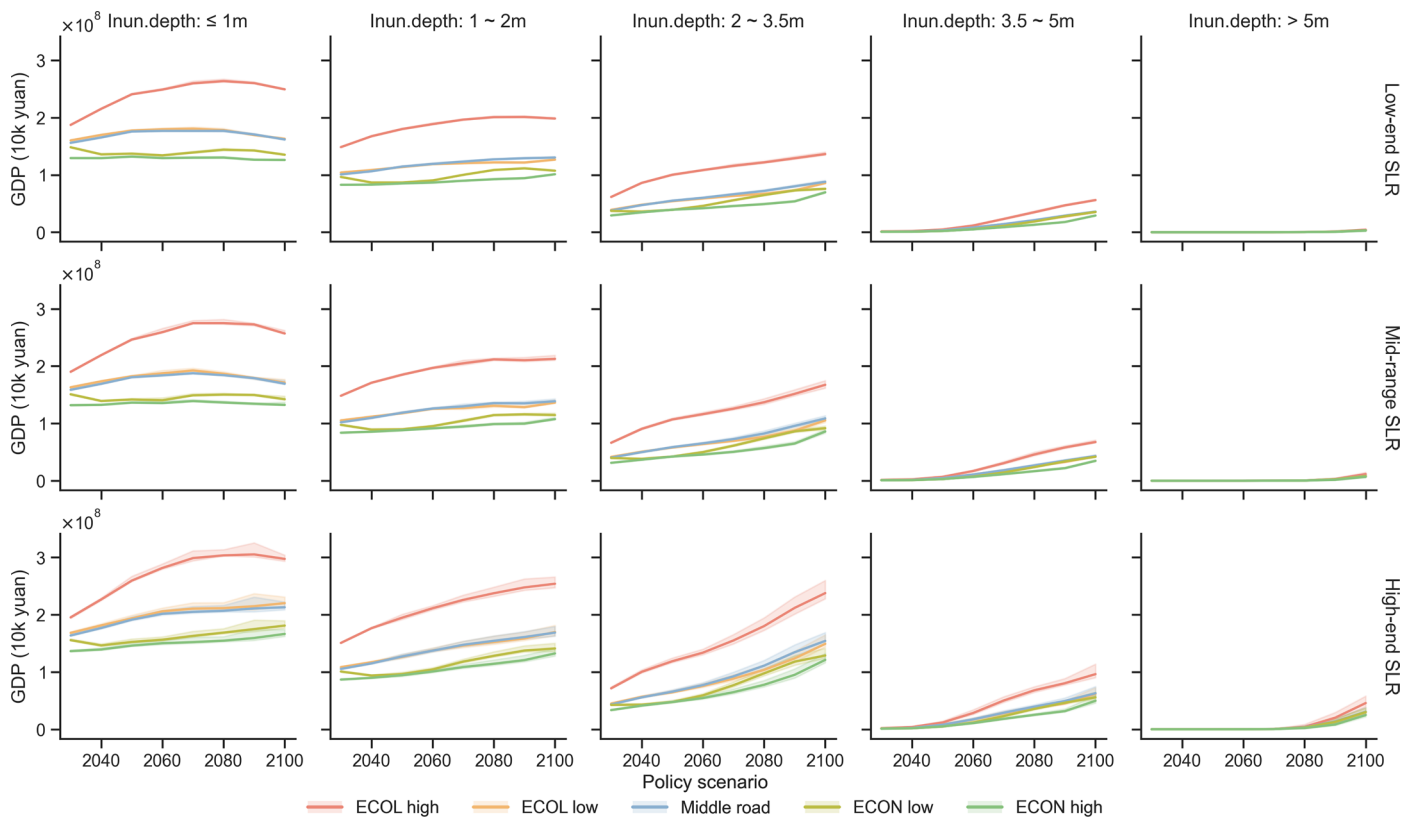
**Extended Data Fig. 7 | Comparison of exposed grain production by inundation depth under different scenarios with current flood protection standards.** Solid lines represent the exposure values for CCEX<sub>10</sub>, and shaded bands indicate

the upper and lower bounds of CCEX<sub>30</sub> and sea-level rise (SLR) scenario with no interaction. CCEX<sub>10</sub> and CCEX<sub>30</sub> indicate, respectively, a 10% and 30% inactive effect between SLR and extreme events.



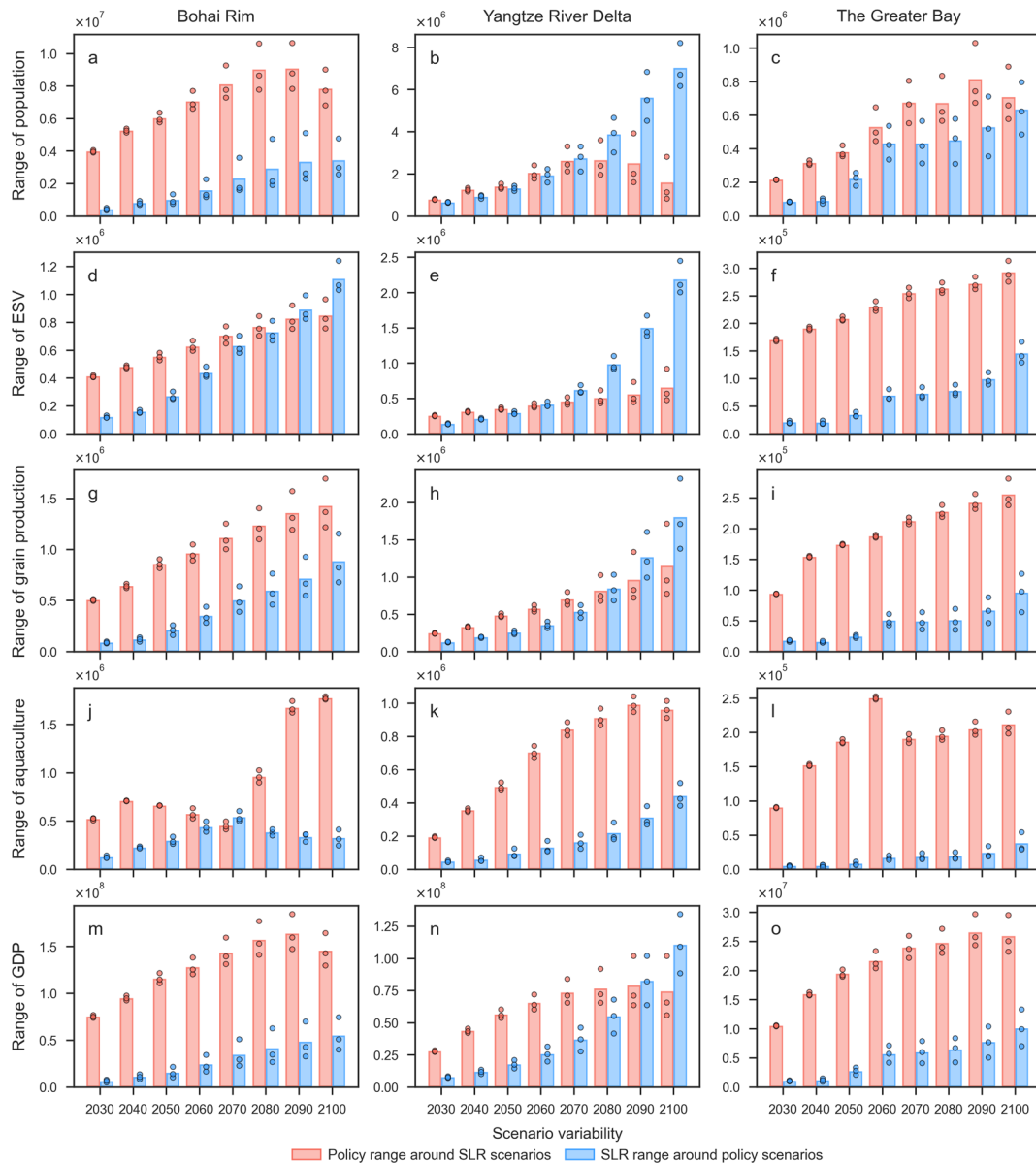
**Extended Data Fig. 8 | Comparison of exposed aquaculture production by inundation depth under different scenarios with current flood protection standards. Solid lines represent the exposure values for CCE<sub>x10</sub>, and shaded**

**bands indicate the upper and lower bounds of CCE<sub>x30</sub> and sea-level rise (SLR) scenario with no interaction. CCE<sub>x10</sub> and CCE<sub>x30</sub> indicate, respectively, a 10% and 30% inactive effect between SLR and extreme events.**



**Extended Data Fig. 9 | Comparison of exposed ecosystem services value (ESV) by inundation depth under different scenarios with current flood protection standards. Solid lines represent the exposure values for CCE<sub>x<sub>10</sub></sub>, and shaded**

**bands indicate the upper and lower bounds of CCE<sub>x<sub>30</sub></sub> and sea-level rise (SLR) scenario with no interaction. CCE<sub>x<sub>10</sub></sub> and CCE<sub>x<sub>30</sub></sub> indicate, respectively, a 10% and 30% inactive effect between SLR and extreme events.**



**Extended Data Fig. 10 | The range of variation for different coastal zone functions in policy scenarios and sea-level rise (SLR) scenarios across China's three strategic zones, assuming current flood protection standards. Left panels (a, d, g, j, m), middle panels (b, e, h, k, n), and right panels (c, f, i, l, o) represent Bohai Rim, Yangtze River Delta, and the Greater Bay, respectively.**

Red bars show decadal variability (range) around SLR scenarios driven by policy; blue bars show decadal variability (range) around policy scenarios driven by SLR. Points represent the range around each of the three scenario combination sets; bar heights indicate the average of the three.

## Reporting Summary

Nature Portfolio wishes to improve the reproducibility of the work that we publish. This form provides structure for consistency and transparency in reporting. For further information on Nature Portfolio policies, see our [Editorial Policies](#) and the [Editorial Policy Checklist](#).

### Statistics

For all statistical analyses, confirm that the following items are present in the figure legend, table legend, main text, or Methods section.

n/a Confirmed

- The exact sample size ( $n$ ) for each experimental group/condition, given as a discrete number and unit of measurement
- A statement on whether measurements were taken from distinct samples or whether the same sample was measured repeatedly
- The statistical test(s) used AND whether they are one- or two-sided  
*Only common tests should be described solely by name; describe more complex techniques in the Methods section.*
- A description of all covariates tested
- A description of any assumptions or corrections, such as tests of normality and adjustment for multiple comparisons
- A full description of the statistical parameters including central tendency (e.g. means) or other basic estimates (e.g. regression coefficient) AND variation (e.g. standard deviation) or associated estimates of uncertainty (e.g. confidence intervals)
- For null hypothesis testing, the test statistic (e.g.  $F$ ,  $t$ ,  $r$ ) with confidence intervals, effect sizes, degrees of freedom and  $P$  value noted  
*Give  $P$  values as exact values whenever suitable.*
- For Bayesian analysis, information on the choice of priors and Markov chain Monte Carlo settings
- For hierarchical and complex designs, identification of the appropriate level for tests and full reporting of outcomes
- Estimates of effect sizes (e.g. Cohen's  $d$ , Pearson's  $r$ ), indicating how they were calculated

*Our web collection on [statistics for biologists](#) contains articles on many of the points above.*

### Software and code

Policy information about [availability of computer code](#)

#### Data collection

Sample points used for predicting land subsidence rates were extracted from figures in previously published, peer-reviewed journal articles using WebPlotDigitizer v4.6 (<https://automeris.io/WebPlotDigitizer>), a validated tool for digitizing graphical data. The original sources from which data were extracted are properly cited in the Supplementary Data 2. For the logistic regression modeling of land suitability, sample points were generated and processed using CLUMondo v1.4.0, a spatially explicit land-use allocation model. The configuration files, model parameters, and derived datasets used in the suitability analysis are available via Figshare at <https://doi.org/10.6084/m9.figshare.29263130>.

#### Data analysis

The CLUMondo model is available on GitHub (<https://github.com/VUEG/CLUMondo>). Python scripts used for projecting land subsidence and generating figures can be accessed via Figshare at <https://doi.org/10.6084/m9.figshare.29263130>. The improved bathtub model, which incorporates hydrological connectivity and attenuation, is available on GitHub ([https://github.com/geoye/attenuated\\_bathtub](https://github.com/geoye/attenuated_bathtub)). ArcGIS Pro is used for analyzing spatial data and creating maps. Additional code supporting the findings of this study is available from the corresponding author upon reasonable request.

For manuscripts utilizing custom algorithms or software that are central to the research but not yet described in published literature, software must be made available to editors and reviewers. We strongly encourage code deposition in a community repository (e.g. GitHub). See the Nature Portfolio [guidelines for submitting code & software](#) for further information.

## Data

Policy information about [availability of data](#)

All manuscripts must include a [data availability statement](#). This statement should provide the following information, where applicable:

- Accession codes, unique identifiers, or web links for publicly available datasets
- A description of any restrictions on data availability
- For clinical datasets or third party data, please ensure that the statement adheres to our [policy](#)

The projected land system maps for five policy scenarios, along with associated validation datasets and sampling points used for projecting land subsidence, are available on Figshare: <https://doi.org/10.6084/m9.figshare.29263130>. Input datasets for CLUMondo simulations are cited throughout the manuscript, with full documentation provided in Supplementary Note 4 and Supplementary Table S4. Sea-level rise (SLR) projections were obtained from the IPCC AR6 database (Zenodo: <https://zenodo.org/records/6382554>), and tide and surge data were sourced from the CoDEC dataset (Zenodo: <https://zenodo.org/records/3660927>). Coastal elevation data (CoastalDEM) were acquired from Climate Central (<https://go.climatecentral.org>), and mean dynamic topography (MDT) data were obtained from AVISO (<https://doi.org/10.24400/527896/a01-2023.003>). Sources for the explanatory variables used in modeling land subsidence are detailed in Supplementary Table S7. All source data supporting the findings of this study are provided with the paper or are publicly available from the cited repositories.

## Research involving human participants, their data, or biological material

Policy information about studies with [human participants or human data](#). See also policy information about [sex, gender \(identity/presentation\), and sexual orientation](#) and [race, ethnicity and racism](#).

Reporting on sex and gender

Reporting on race, ethnicity, or other socially relevant groupings

Population characteristics

Recruitment

Ethics oversight

Note that full information on the approval of the study protocol must also be provided in the manuscript.

## Field-specific reporting

Please select the one below that is the best fit for your research. If you are not sure, read the appropriate sections before making your selection.

Life sciences  Behavioural & social sciences  Ecological, evolutionary & environmental sciences

For a reference copy of the document with all sections, see [nature.com/documents/nr-reporting-summary-flat.pdf](https://www.nature.com/documents/nr-reporting-summary-flat.pdf)

## Ecological, evolutionary & environmental sciences study design

All studies must disclose on these points even when the disclosure is negative.

Study description

This study addresses three key applications of sampling techniques in spatial analysis: (1) Integrating sampling with machine learning to improve long-term land use classification accuracy using remote sensing and historical land-use data; (2) Combining sampling and machine learning approaches to model spatially explicit land subsidence rates, based on observed subsidence points and explanatory environmental variables; (3) Applying spatial sampling methods to assess local land-use suitability within a logistic regression framework in the CLUMondo land system model, enabling policy-driven scenario projections. Sampling strategies in each application were tailored to the spatial resolution, data availability, and modeling requirements, and are described in detail in the Methods and Supplementary Information.

Research sample

The study employed distinct sampling strategies for three core components: (1) Land use classification: A total of 4,700 sample points were manually identified to document annual land cover types across China's coastal zone from remote sensing imagery. The sampling ensured temporal and spatial representativeness across diverse land systems. (2) Land subsidence modeling: A total of 6,203 sample points were compiled from published sources and field records, comprising 4,417 subsidence points and 1,786 non-subsidence points. These were used to train and validate machine learning models predicting spatial patterns of subsidence. (3) Land suitability analysis (CLUMondo): For logistic regression modeling of land system suitability, a random sample of 30% of grid cells within the study region was used to reduce computational burden while maintaining statistical power and geographic coverage. Full details on the spatial resolution, source data, and sampling rationale are provided in the Methods section and Supplementary Information.

Sampling strategy

(1) Land use classification: 80% of the samples were used to train a Random Forest classifier, while the remaining 20% were reserved for accuracy assessment. To mitigate sampling bias, random iterations were performed 20 times, and the iteration with the highest

accuracy was selected for the final prediction.(2) Land subsidence rate modeling: A nested cross-validation (CV) approach was applied. In the inner loop, a 5-fold GridSearchCV (from Python's scikit-learn package) was used to optimize hyperparameters and minimize overfitting. In the outer loop, a 10-fold random CV provided an unbiased estimate of the model's generalization performance. Each Random Forest regressor was executed 20 times with varying training, testing, and validation sample distributions. (3) Suitability regression in CLUMondo: A stratified sample comprising 30% of all cells in the study region was used for logistic regression analysis to quantify relationships between specific land system types and explanatory factors. To reduce spatial autocorrelation, a minimum separation of 2 km (2 pixels) was enforced between sampled cells. The logistic regression dataset maintained a balanced sample, including an equal number of presence and absence points for each land use type.

## Data collection

Land use classification data were collected from two primary sources: (1) Field surveys conducted in ten Chinese coastal provinces (Liaoning, Tianjin, Hebei, Shandong, Jiangsu, Shanghai, Zhejiang, Fujian, Guangdong, and Guangxi); and (2) Visual interpretation of high-resolution historical imagery from Google Earth. These sample points ( $n = 4,700$ ) were used to train a Random Forest classifier in Google Earth Engine for generating annual land use maps.Land subsidence data ( $n = 6,203$ ) were digitized from 40 peer-reviewed journal articles and international datasets using WebPlotDigitizer (v4.6). The extracted data were georeferenced in ArcMap 10.8 based on geographic coordinates or map overlays provided in the original publications.Land suitability data for use in the CLUMondo model were derived by randomly sampling 30% of grid cells across the study region. Environmental and socio-economic input layers used in the logistic regression were compiled from authoritative, publicly available datasets, with full source information provided in Supplementary Table S4.

## Timing and spatial scale

Temporal scope: The study includes both historical and future projections. Historical land use classification was conducted using Landsat satellite imagery spanning 1990–2020. Future land system changes were projected at decadal intervals from 2020 to 2100 under three Shared Socioeconomic Pathways (SSP126, SSP245, and SSP585) and five additional policy-driven scenarios. Spatial scope: The spatial extent of the study includes all coastal prefecture-level cities and municipalities in mainland China, including Hong Kong, Macao, and Hainan Province.Land system simulations were performed at a spatial resolution of 1 km<sup>2</sup>, while coastal flooding and inundation analyses were conducted at a finer resolution of 1 ha (100 m × 100 m) to capture localized hydrological impacts.

## Data exclusions

Pixels labeled as 'Nodata' were excluded from all spatial analyses.In land subsidence modeling, the following exclusions and adjustments were applied to ensure data quality and minimize spatial or statistical bias: (1) Non-subsiding locations (subsidence rates < 0 mm/year) were assigned a value of 0 mm/year to avoid introducing negative values into the regression model. (2) Duplicate or overlapping sampling points within 1 km grid cells were removed to reduce spatial redundancy and avoid overrepresentation of specific locations. (3) The number of zero-subsidence points was downsampled to address class imbalance and prevent model bias toward stable (non-subsiding) areas.

## Reproducibility

To ensure reproducibility across all analyses: (1) Land system classification: The seed parameter was set in the Random Forest classifier within Google Earth Engine to control data splits and ensure consistent classification results across repeated runs. (2) Land subsidence rate modeling: The random\_state parameter was applied during cross-validation and regression procedures in Python (scikit-learn) to maintain reproducibility of results. (3) Suitability regression in CLUMondo: The randomly selected training samples used in logistic regression were saved to disk within CLUMondo v1.4.0 to ensure consistency across model calibration and future re-runs. (4) Land system model calibration and validation: The CLUMondo model was calibrated using logistic regression on historical land system data and validated by comparing simulated outcomes with observed land system maps from 2010 to 2020. The model achieved an overall accuracy of 72.18% and a Figure of Merit (FoM) of 0.278, demonstrating good agreement with real-world land system changes.

## Randomization

(1) Land use classification: Training data were randomly sampled 20 times to minimize the influence of sample distribution on classification outcomes and to ensure the robustness of the Random Forest classifier implemented in Google Earth Engine. (2) Land subsidence rate modeling: A nested cross-validation procedure with 20 repeated experiments was used in the machine learning workflow to generate unbiased, generalizable predictions and reduce overfitting. (3) Suitability regression in CLUMondo: A random selection of 30% of grid cells across the study region was used to fit logistic regression models quantifying relationships between land system types and explanatory variables. To further reduce spatial sampling bias, a minimum distance of 2 km between samples was enforced, and balanced sampling across land system types was applied to avoid overrepresentation of dominant classes.

## Blinding

This study used fully objective, data-driven methods with no subjective assessments; blinding was not applicable.

Did the study involve field work?  Yes  No

## Field work, collection and transport

## Field conditions

Fieldwork was conducted in the coastal zones of China, regions characterized by diverse environmental conditions. These areas are influenced by various climatic factors, such as monsoonal weather patterns and occasional extreme events like typhoons. The coastal zones also experience significant human activity, including urbanization, industrial development, and agricultural or aquacultural practices. During the fieldwork, sample points for land use classification were collected through photography to document land cover types, as well as interviews to gather information on land use changes and local perceptions of coastal flooding risks.

## Location

Fieldwork was conducted across ten coastal provinces and municipalities in China: Liaoning, Tianjin, Hebei, Shandong, Jiangsu, Shanghai, Zhejiang, Fujian, Guangdong, and Guangxi. These regions were selected due to their significant coastal land system transformations and high exposure to sea-level rise and coastal flooding, offering a representative gradient of coastal environmental and socio-economic conditions from north to south.Field sampling and semi-structured interviews were conducted in specific locations within these areas, including but not limited to: (1) Yingkou and Panjin (Liaoning); (2) Tianjin Municipality; (3) Caofeidian (Tangshan) and Huanghua (Cangzhou), Hebei; (4) Qingdao (Shandong); (5) Ganyu (Lianyungang) and Dafeng (Yancheng), Jiangsu; (6) Zhenhai (Ningbo) and Wenling (Taizhou), Zhejiang; (7) Xiamen (Fujian); (8) Shantou and Guangzhou (Guangdong).These sites cover diverse coastal geomorphologies, land use pressures, and development patterns, forming a robust empirical foundation for the study.

Access & import/export

Disturbance

## Reporting for specific materials, systems and methods

We require information from authors about some types of materials, experimental systems and methods used in many studies. Here, indicate whether each material, system or method listed is relevant to your study. If you are not sure if a list item applies to your research, read the appropriate section before selecting a response.

### Materials & experimental systems

| n/a                                 | Involvement in the study                               |
|-------------------------------------|--|
| <input checked="" type="checkbox"/> | <input type="checkbox"/> Antibodies                    |
| <input checked="" type="checkbox"/> | <input type="checkbox"/> Eukaryotic cell lines         |
| <input checked="" type="checkbox"/> | <input type="checkbox"/> Palaeontology and archaeology |
| <input checked="" type="checkbox"/> | <input type="checkbox"/> Animals and other organisms   |
| <input checked="" type="checkbox"/> | <input type="checkbox"/> Clinical data                 |
| <input checked="" type="checkbox"/> | <input type="checkbox"/> Dual use research of concern  |
| <input checked="" type="checkbox"/> | <input type="checkbox"/> Plants                        |

### Methods

| n/a                                 | Involvement in the study                        |
|-------------------------------------|---|
| <input checked="" type="checkbox"/> | <input type="checkbox"/> ChIP-seq               |
| <input checked="" type="checkbox"/> | <input type="checkbox"/> Flow cytometry         |
| <input checked="" type="checkbox"/> | <input type="checkbox"/> MRI-based neuroimaging |

## Plants

Seed stocks

Novel plant genotypes

Authentication